Thesis for the degree of Doctor of Philosophy

Alcohol Flexible Dual-Fuel Direct Injection Engine

Challenging the HD-Diesel engine with a fully fuel flexible concept

Michael Saccullo

Department of Mechanics and Maritime Sciences
CHALMERS UNIVERSITY OF TECHNOLOGY
Göteborg, Sweden 2020

Alcohol Flexible Dual-Fuel Direct Injection Engine
Challenging the HD-Diesel engine with a fully fuel flexible concept
MICHAEL SACCULLO
ISBN 978-91-7905-386-4

© MICHAEL SACCULLO, 2020.

Doktorsavhandlingar vid Chalmers tekniska högskola
Ny serie nr 4853
ISSN 0346-718X

Department of Mechanics and Maritime Sciences
Chalmers University of Technology
SE–412 96 Göteborg, Sweden
Telephone + 46 (0) 31 – 772 1000

Cover: Dual-Fuel Engine in action by Annabel Jerre

Typeset by the author using LaTeX.

Printed by Chalmers Reproservice
Göteborg, Sweden 2020

Abstract

Laws concerning emissions from HD internal combustion engines are becoming increasingly stringent in terms of local emissions and emissions concerning global warming such as lowering tailpipe CO_2. New engine technologies are needed to satisfy these new requirements and to reduce fossil fuel dependency and increase renewable fuels in the transportation sector. One way to achieve both objectives can be to partially replace fossil fuels with alternatives that are sustainable with respect to emissions of greenhouse gases and engine out particulates. Also a decrease in NOx can be achieved. Suitable candidates are ethanol or methanol.

The thesis presented here summarizes results from publications and additional results presented here with the aim to investigate the possible advantages of combusting low carbon alcohol fuels in dual-fuel configuration in a HD Diesel engine - in particular, the potential to greatly reduce particulate emissions and thereby bypass the soot-NOx tradeoff and lowering tailpipe CO_2 emissions. It was complimented by additional results presented in the kappa itself.

Ethanol sprays were studied in a high pressure/temperature spray chamber at typical engine condition with gas densities of about 27 kg/m^3 at around 550 °C and around 60 bar. Spray parameters, such as the liquid cone angle, liquid penetration length and vapor penetration at injection pressures up to 2200 bar, were investigated. The characterization of those sprays was followed by an investigation focusing on the combustion of alcohol fuels in a single cylinder engine. Methanol, ethanol and E85 were chosen, but because of their poor auto-ignition properties, a pilot Diesel injection was used to initiate the combustion process. One of the alcohol fuels and Diesel were injected directly but separately, necessitating the use of two separate common rail systems together with a newly designed cylinder head and adapted injection nozzles. The dual fuel system's combustion properties were compared to those of pure Diesel with the same dual injection strategy. The injection pressure on the alcohol side were varied up to 2000 bar and investigations were carried out at low, medium and high speed-load points, with and without EGR. The investigated low carbon fuels outperformed Diesel under all tested conditions in terms of thermal efficiency and indicated specific ($\eta_{f,ig}$), NOx, soot and CO_2 emissions. $\eta_{f,ig}$ was increased by up to 3.5 %-points and simultaneously soot emissions were lowered by a factor of 40 or more and NOx by 20 %. $ISCO_2$ emissions were down by up to 25 %. The fuel substitution ratio was over 95 % and the combustion stability was not compromised.

Keywords: Dual-fuel, Ethanol, Methanol, E85, Heavy duty engine, Fuel spray, Dual-direct injection, Diffusion combustion.

Acknowledgments

First and foremost I want to thank my main supervisor, Ingemar Denbratt, and my co-supervisor, Anders Karlsson, for giving me the opportunity to work on this PhD project. It was great fun working and researching at Chalmers, but also presenting the work on conferences around the world. Thank you for the support and the many fruitful discussions during the course of my PhD.

Further my thanks goes to all Chalmers lab engineers that helped me with small, but often bigger problems around the test rig. Thank you, Robert Buadu for helping with everything related to electrical systems and more, Anders Mattsson for always giving a helping hand and finding practical solutions quickly, Patrik Wåhlin for your support in the spray lab and the many, many interesting talks and helping me understand this world a bit better and Alf Magnusson for helping with great philosophical advise and the good times on the football pitch.

A very special thanks goes to Timothy Benham. Tim, it was a great to have such kind, skilled and experienced colleague to learn from. It was a pleasure working with you and quite fun to solve all the technical difficulties and riddles the engine lab gave us. Thank you for the great support and all the interesting discussions.

I must also thank my colleagues with whom I have worked on the project, including Jan Eismark, Johan Engström, Ingemar Magnusson, Anders Pärsson and Niclas Wenneberg among others from Volvo GTT. I am deeply indebted to you for all your support, especially on technical issues, and for many fruitful and inspiring discussions.

A special thanks goes to my two colleagues Andreas and Vignesh, with whom I have the honour of sharing an office and who quickly became my friends. Thank you for all the good times we had in the office, but also outside. Especially, the regular Friday afterworks were awesome. I could not have wished for better office mates.

I also have to thank Jelmer, with whom I didn’t share an office, but we had great times at Chalmers and outside, especially during a road-trip from Detroit to San Francisco after a conference. Thank you Zhiqin for your help in the lab, but also for taking care of Zelda while I was not in Göteborg. Last but not least I want to thank all my other colleagues and friends at the CaPS and Chalmers. At this point I have to thank Elenor for your administrative and moral support during the last 5 years.

Further I want to thank my girlfriend Selin and my family and friends at home for their love and encouragement.

Funding from the Swedish Energy Agency is gratefully acknowledged.

Michael Saccullo
Göteborg, October 2020

List of Publications

This thesis is based on the following appended papers:

Paper I. Michael Saccullo, Mats Andersson, Jan Eismark and Ingemar Denbratt. *"High Pressure Ethanol Injection under Diesel-like Conditions."* in SAE WCX Detroit (2017).

Paper II. Michael Saccullo, Timothy Benham and Ingemar Denbratt. *"Dual Fuel Methanol and Diesel Direct Injection HD Single Cylinder Engine Tests."* in SAE WCX Detroit (2018).

Paper III. Michael Saccullo, Timothy Benham, Bengt Johansson and Ingemar Denbratt. *"CI Methanol and Ethanol combustion using ignition improver."* in JSAE/SAE Powertrains, Fuels and Lubricants International Meeting in Kyoto (2019).

Paper IV. Michael Saccullo, Timothy Benham and Ingemar Denbratt. *"Alcohol flexible HD Single Cylinder Diesel Engine Tests with Separate Dual High Pressure Direct Fuel Injection."* in Fuel, under revision (2020).

Paper V. Andreas Nygren, Michael Saccullo and Anders Karlsson. *"CFD Modeling of a Direct Injection Dual Fuel Engine."* prepared for Fuel, (2020).

Additional contributions not appended:

Paper VI. Carlo Beatrice, Ingemar Denbratt, Gabriele di Blasio, Giuseppe Di Luca, Roberto Ianello and Michael Saccullo *"Experimental Assessment on Exploiting Low Carbon Ethanol Fuel in a Light-Duty Dual-Fuel Compression Ignition Engine."*, in Applied Sciences, under revision (2020).

List of Acronyms

$\eta_{f,ig}$ – Indicated Gross Thermal Efficiency
ϕ – Equivalence Ratio
aRoHR – Apparent Rate of Heat Release
aTDC – After Top Dead Center
bTDC – Before Top Dead Center
CA50 – Crank Angle where 50 % fuel mass was burned, also comubstion phasing
CA90 – Crank Angle where 90 % fuel mass was burned
CAD – Crank Angle Degree
CCF – Central Composite Face
CFD – Computational Fluid Dynamics
CI – Compression Ignition
CMOS – Complementary Metal–Oxide–Semiconductor
CO – Carbon Monoxide
CO2 – Carbon Dioxide
CR – Compression Ratio
DDFS – Direct Dual Fuel Stratification
DoE – Design of Experiments
DUR – Combustion duration (CA90 - SOC)
E85 – Ethanol and Gasoline, 85 % to 15 % by weight
ECU – Engine Control Unit
EGR – Exhaust Gas Recirculation
EOI – End of Injection
FSR – Fuel Substitution Ratio
GHG – Greenhouse Gases
HC – Hydrocarbon
HCCI – Homogeneous Charge Compression Ignition
HD – Heavy Duty
HP/HT – High Pressure & Hight Temperature
HR – Heat Release

ISCO – Indicated Specific Carbon Monoxide Emission
ISCO2 – Indicated Specific CO2 Emissions
ISHC – Indicated Specific Hydrocarbon Emissions
ISNOx – Indicated Specific NOx Emissions
ISSOOT – Indicated Specific SOOT Emissions
LD – Light Duty
LTC – Low Temperature Combustion
Nm – Newtonmeter
Nox – Nitrous Oxides
PCCI – Premixed Charge Compression Ignition
PFI – Port fuel Injection
PPC – Partially Premixed Combustion
Q2 – Estimate of Regression Models future predictions
R2 – Regression Model fit
RCCI – Reactivity Controlled Compression Igintion
rpm – rounds per minute
RSC – Rig Stability Check
SCE – Single Cylinder Engine
SOC – Start of Combustion
SOI – Start of Injection
TDC – Top Dead Center
UV – Ultra Violet

Contents

Abstract iii

Acknowledgments v

List of Publications vii

List of Acronyms ix

I Introductory chapters 1

1 Introduction 3
1.1 Motivation . . . 3
1.2 Background . . . 5
1.3 Objectives and Research Questions . . . 5

2 Combustion Strategies in CI Engines 7
2.1 The soot-NOx trade-off . . . 7
2.2 Combustion Strategies . . . 7
  2.2.1 Conventional Diesel combustion . . . 8
  2.2.2 Low Temperature Combustion (LTC) . . . 8
2.3 Dual-Fuel Combustion . . . 10
  2.3.1 Definitions . . . 10
  2.3.2 Renewable Fuels in Dual-Fuel engines . . . 10
  2.3.3 Single-fuel mixture direct injection (DI) . . . 11
  2.3.4 PFI and DI . . . 11
  2.3.5 Direct Dual-Fuel Combustion . . . 11
  2.3.6 Fuel sprays . . . 12

3 Experimental Set-up 13
3.1 Fuels and Fueling system . . . 13
3.2 Spray Chamber Experiments . . . 13
  3.2.1 Optical setup . . . 14
  3.2.2 Measurements and spray evaluation . . . 15
3.3 Engine Experiments . . . 17
  3.3.1 Data acquisition and handling . . . 19

3.3.2 Methods 20

4 Summary of Publications **23**
4.1 Paper I 23
4.2 Paper II 24
4.3 Paper III 24
4.4 Paper IV 25
4.5 Paper V 25

5 Results and Discussions **27**
5.1 Rig Stability Check (RSC) 27
5.2 Design of Experiments 30
5.2.1 1262 rpm 172 Nm 30
5.2.2 1262 rpm 172 Nm EGR 37
5.2.3 Summary of DoE results 40
5.3 Wave Piston Results 41
5.4 Influence of the Hydraulic Flow on Methanol Dual-Fuel Combustion . 43
5.4.1 1262 rpm 172 Nm 43
5.4.2 871 rpm 86 Nm 45
5.4.3 1400 rpm 305 Nm 47
5.4.4 Energy balances 48

6 Conclusions **51**
6.1 Conclusions from spray experiments 51
6.2 Conclusions from SCE Experiments 51
6.3 Conclusions summary 53

7 Outlook **55**

Bibliography **57**

II Appended papers **63**

Part I

Introductory chapters

Chapter 1

Introduction

1.1 Motivation

Historically, the transportation of people and goods has always been driven by innovation. From the invention of the wheel over the steam engine towards the internal combustion engine (ICE) and its electric counterpart or complement, the improvement of already existing or development of new technologies were central for the development of the society as such. Since the industrial revolution and invention of the steam engine, the combustion of fossil fuels has increased, causing many challenges. Nowadays, more products, goods and people are transported globally than ever before, not only due to the increased global population [33]. The urbanization process, global markets and changes in supply chains within industry are shaping the transportation sector of today. Additionally, changes in customer behavior, especially online-shopping, indicate an increased demand in the freight transportation sector [55]. An investigation ordered by the European Commission predicted an increase of road freight traffic by 57 % in 2050 compared with 2010 as shown in Figure 1.1a.

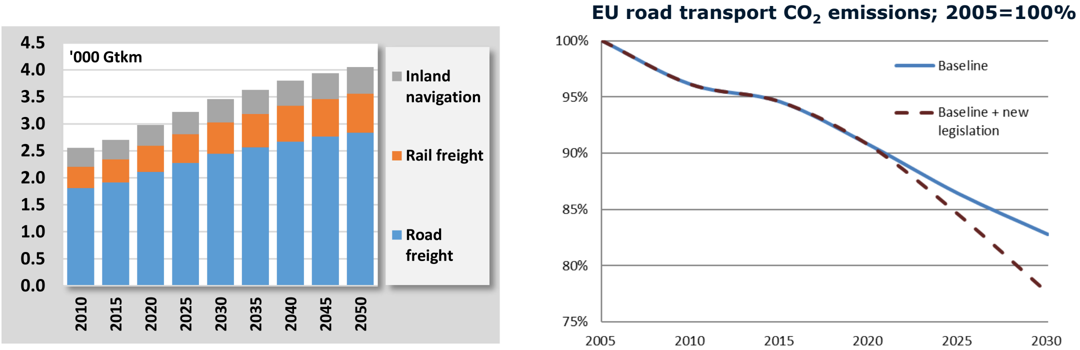

(a) Future trends in freight transportation as predicted by the EU according to mode.

(b) Fleet average reduction targets of tailpipe CO_2 emission from HD.

Figure 1.1: Prediction of the development of road transportation and fleet average targets for tailpipe CO_2 emissions reduction of the EU commission[13, 12].

The main challenge is the simultaneous reducing tailpipe CO_2 emissions through fleet average emission targets and at the same time an increase in freight transportation sector is expected.

Accompanying these challenges, emissions of greenhouse gases (GHGs) and local pollutants, such as particulates, nitrous oxides (NOx) and hydrocarbons (HC), have also increased because most goods in Europe are transported using trucks powered by a Diesel ICE. Increased emissions of particulates and NOx increase the risk of severe health-related issues, especially those affecting the cardiovascular system, as noted by the Health Effects Institute in a special report on emissions from Diesel engines [18]. Globally, the use of primary energy from fossil fuels is still rising, either through the direct combustion of fossil fuels or indirectly by alternative propulsion systems that rely on electricity generated from fossil fuels. There is now an almost undisputed global consensus that fossil fuel consumption must be reduced to control GHG emissions, and thereby counter the challenges of global warming [19]. There is no avoiding the fact that all emissions from ICEs must be reduced significantly to meet these challenges, and it is almost certain that more stringent emissions regulations will be introduced in the near future to improve urban air quality and reduce GHG emissions arising from fossil fuel combustion. Some such regulations have already been introduced, as exemplified by the local bans on Diesel engines without particulate filters in some German cities [6]. In 2016, the European Commission summarized its goals regarding emissions from the transportation sector as follows:

"by midcentury, greenhouse gas emissions from transport will need to be at least 60 % lower than in 1990 and be firmly on the path towards zero. Emissions of air pollutants from transport that harm our health need to be drastically reduced without delay." [11]

In 2019, the EU commission created a new emission legislation and formulated an ambitious goal for CO_2 emission reduction in the HD sector. The new regulation does not only target local emissions, but puts a great focus on reducing GHG emissions from HD applications. The main targets are formulated as, each manufacturer fleet has to reduce tailpipe CO_2 emissions compared to baseline 2019 emissions [50]:

- by 15 % in 2025
- by 30 % in 2030

Those targets are reflected by Figure 1.1b and also include that renewable sources should cover 14 % of the fuel consumption in 2030 [12].

Consequently, there is an urgent need to implement new engine technologies that can reduce the impact of these harmful substances and allow vehicle manufacturers to comply with future regulations. Similar legislative interventions designed to spur the uptake of environment-protecting technologies and curb emissions of pollutants have already been successfully implemented, as demonstrated by the ban on CFC production and use to halt the growth of the hole in the ozone layer, the introduction of exhaust gas filter systems to prevent acid rain by trapping sulfur dioxide emissions from coal- and lignite-fuelled power plants, and the ban on leaded gasoline additives [27, 26].

1.2 Background

To achieve the goals of reducing GHG and local emissions from heavy duty (HD) ICEs, it will be necessary to develop affordable emissions-reducing technologies that can be taken up quickly by the market. The fuel efficiency and engine out emission profiles of HD Diesel engines have improved greatly in recent years, and exhaust gas aftertreatment systems have been introduced to further reduce tailpipe emissions (at the cost of slightly reducing gains in engine efficiency and performance). However, given the expected growth in the transportation sector and need to reduce emissions further, greater efforts will be required. One possible way of reducing emissions from HD ICEs is to operate them using alcohol-based alternative fuels that can be produced from renewable sources. Experiments with alcoholic fuels such as methanol and ethanol have yielded high thermal combustion efficiencies and promisingly low engine out soot emissions. The benefits of reduced tailpipe CO_2 emissions are important to fulfil regulatory requirements set by EU legislation. It does not differentiate between CO_2 from fossil and renewable sources, due to the tank-to-wheel approach. But in order to achieve a greater reduction of GHG emissions the complete system has to be included in a well-to-wheel investigation. An alcohol generated in a sustainable fashion from renewable sources can reduce those emissions from a global perspective.

1.3 Objectives and Research Questions

The work presented in this thesis explores a new dual-fuel combustion system that combines an injection technique similar to a direct injection dual-fuel system with a combustion strategy resembling that used in conventional Diesel engines. The main objective of the work was to use dual-fuel direct injection strategies to combine the established advantages of Diesel engines, such as high fuel efficiency, with those of alcohol fuels, such as low particulate and tailpipe CO_2 emissions. The initial primary objectives were to establish a proof of concept and validate the use of existing Diesel injection systems for high pressure alcohol injection. An additional early goal was to characterize the liquid penetration length, liquid cone angle and vapor phase distribution of direct injected alcohol sprays to determine the similarities and differences between alcohol and Diesel sprays under conditions resembling those occurring in Diesel engines. The results of the initial spray experiments were used to guide design of engine experiments performed on a HD engine using methanol, ethanol and E85 with pilot Diesel injection to facilitate ignition. The main objectives during the engine tests were to establish stable running conditions and determine the values of important combustion parameters, engine-out emissions levels and fuel efficiencies at different speed-load points. The results obtained in these experiments were compared to reference data obtained by burning pure Diesel fuel in the same engine. The results obtained are being used to guide and validate computational fluid dynamics (CFD) simulations. The main aim was to develop a powertrain system that could handle renewable alcohol fuels in an efficient manner, and thereby reduce CO_2 emissions.

The overall goal of the project was to develop a HD engine concept that could be operated on renewable fuels with the following attributes:

- Higher efficiency than with conventional Diesel, i.e., above 48 %.
- Reduction of GHG emissions by 90 % or more using renewable fuels by adopting a well-to-wheel approach.
- Higher load and power density than a conventional Diesel engine.
- Potential for low emissions to comply with future regulatory measures such as discussions on EURO IV standards.

For the sake of convenience and to facilitate comparisons to existing engines, the experimental engine comprised components from production engines wherever possible. From the above objectives, the following research questions were formulated:

- **Is it possible to have a true alcohol flexible dual-fuel combustion system?**
- **What advantages and challenges, connected to the alcohol flexible dual-fuel direct injection engine, can be identified from experimental studies?**
- **How large is the carbon dioxide CO_2, PM and NOx reduction potential from a flexfuel engine run on various alcohol fuels compared with Diesel?**

Chapter 2

Combustion Strategies in CI Engines

This chapter presents the basic issues that give rise to problematic and unwanted emissions from HD Diesel engines and outlines recent progress in the development of new combustion regimes and alternative fuels.

2.1 The soot-NOx trade-off

The basic operating principles of Diesel engines and the processes of Diesel fuel combustion are well understood after many years of research, and are summarized in detail in texts such as Heywood's "Internal Combustion Engine Fundamentals" [17]. This section briefly reviews some of the principles behind the techniques developed to address the problems of current Diesel engines. Figure 2.1 shows the correlation between the two main local emissions from a conventional Diesel engine, soot and NOx. It also shows how they respond to changes in the local equivalence ratio (ϕ), local combustion temperature, and residence time. The figure illustrates the so-called soot-NOx trade-off, which exists because soot particles are mainly generated in fuel-rich zones at temperatures between 1800 K and 2400 K when the local ϕ is greater than 2. Better fuel mixing and reductions in ϕ that make the combustion process leaner tend to significantly increase the temperature of combustion. This reduces soot formation but also promotes the main mechanism of thermal NOx formation, i.e., the Zeldovich mechanism, which requires combustion temperatures above 2000 K and a nitrogen-rich environment [58]. The key steps in this mechanism are as follows:

$$O + N_2 \rightleftharpoons NO + N \tag{2.1}$$

$$N + O_2 \rightleftharpoons NO + O \tag{2.2}$$

2.2 Combustion Strategies

In Figure 2.1, the main combustion strategies and their respective operating conditions are presented. Below, is a short introduction into the different strategies and current

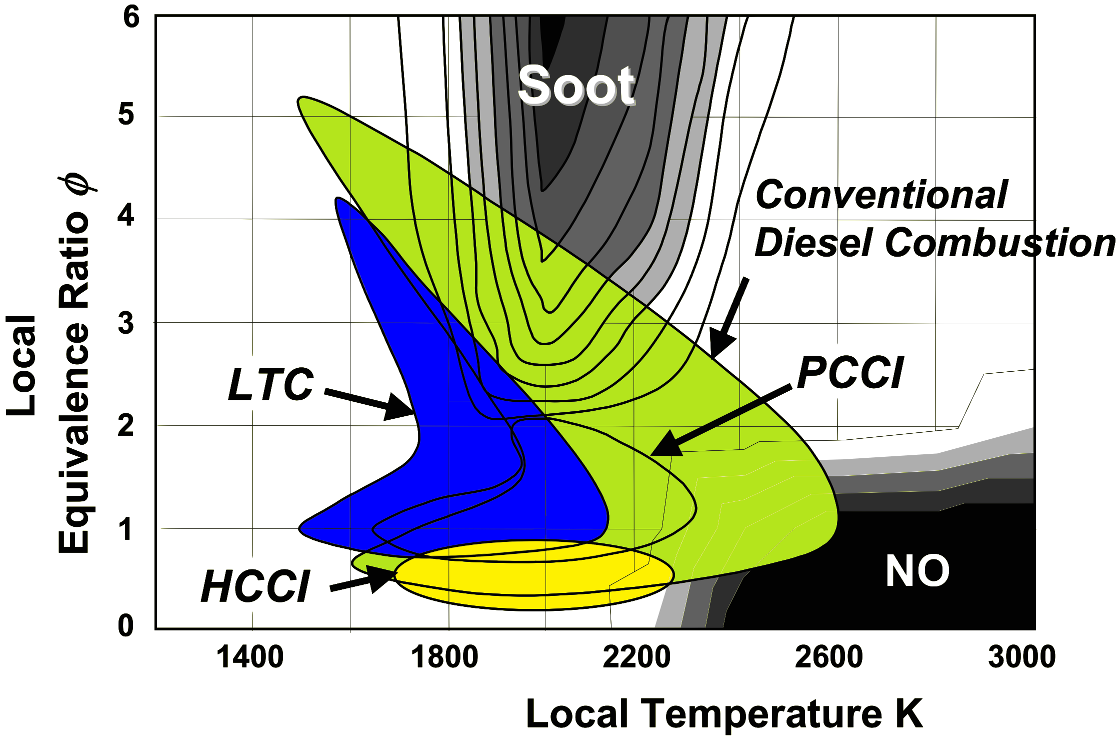

Figure 2.1: Soot-NOx trade-off for different Diesel combustion regimes, LTC: Low temperature combustion; PCCI: Premixed charge compression ignition; HCCI: Homogeneous charge compression ignition. adapted from Neely et.al [31, 20, 1], printed with permission of SAE International.

developments aimed at avoiding the soot-NOx trap. Figure 2.2 shows the different injection strategies available for the different combustion types.

2.2.1 Conventional Diesel combustion

The green area in Figure 2.1 corresponds to the operating conditions for conventional Diesel combustion. Within this region, soot and NOx formation can be tuned by adjusting various engine operating parameters, such as the injector nozzle configuration, injection timing and injection pressure, or the level of exhaust gas recirculation (EGR). The latter reduces in-cylinder temperatures and oxygen levels, and thus reduces NOx formation but promotes soot formation.

2.2.2 Low Temperature Combustion (LTC)

Much research in recent years has focused on the development of LTC concepts that simultaneously reduce soot and NOx formation [2, 38, 32]. The region colored in blue in Figure 2.1 corresponds to LTC operating conditions. In LTC, large amounts of EGR are used to cool the combustion process, leading to increased HC emissions. This is a major disadvantage because it also tends to increase CO emissions at high loads. This due to the cylinder temperature dropping quickly under the temperature

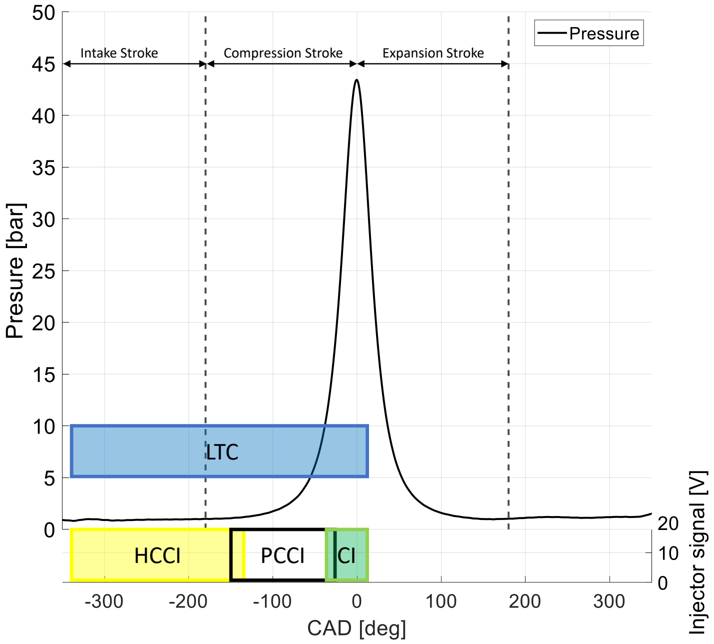

Figure 2.2: Different injection strategies for Homogeneous charge compression ignition (HCCI), premixed charge compression ignition (PCCI) and the standard CI.

threshold for OH radical formation at 1400 K during the expansion stroke, which is necessary for the oxidation of CO and HC. This problem can be alleviated to some extent by using alternative fuels that produce lower GHG, soot and NOx emissions [51]. The two remaining regions can be seen as variants of LTC. Homogeneous charge compression ignition (HCCI) and premixed charge compression ignition (PCCI) are two ways to reduce the in-cylinder temperature and combust leaner mixtures. The charge mixture preparation for HCCI is in most cases categorized by an external charge preparation. It often corresponds to a strategy involving port injection of low cetane fuels. HCCI can simultaneously reduce soot and NOx engine out emissions but achieves comparatively low efficiency and responsiveness to load changes [7]. PCCI often requires in-cylinder charge preparation, with fuel injections occurring early during the intake stroke. This combustion mode evolved from HCCI with the main difference in the level of air-fuel mixing. Two recent review studies focusing on LTC and the effects different fuels have on performance and emissions highlighted the following advantages [35, 21]:

- In general, LTC can improve fuel efficiency whilst reducing NOx and soot emissions simultaneously.
- The dimensioning of exhaust gas aftertreatment systems can be reduced, decreasing the use of materials.
- Using renewable and sustainable biofuels reduces the overall CO_2 emissions in a well-to-wheel perspective.

However, LTC still has many challenges such as

- Higher HC and CO emissions.
- Limited load range due to the need for knocking control at higher loads.
- Ignition timing and combustion control has to be improved.
- Combustion noise and stability.

2.3 Dual-Fuel Combustion

2.3.1 Definitions

The term flexible Dual-Fuel can be interpreted in different ways. Therefore, it is defined here in order to avoid misunderstanding. The term was chosen to describe the combustion of an igniter fuel, here Diesel and a low carbon fuel, here methanol, ethanol or E85. The liquid fuels were not blended at any time during the process and were stored in separated tanks. It has to be pointed out that at no point the engine was operated on either only Diesel or alcohol fuel. The term flexible dual-fuel was often referred to by dual-fuel.

2.3.2 Renewable Fuels in Dual-Fuel engines

Because of the limited scope for reducing the emissions of HD engines burning fossil Diesel, there is considerable interest in biofuels and other sustainable alternative fuels such as Diesel surrogates produced by the Fischer-Tropsch synthesis in reactors powered by electricity from renewable sources, e.g., wind or solar power [15]. All these fuels seem to be suitable alternatives to fossil Diesel. A lot of research has focused on alcohol-based fuels with low cetane numbers [3, 16]. Unfortunately, the low cetane numbers of alcohols give rise to long ignition delays and poor auto-ignitability when used as Diesel substitutes under conventional Diesel engine operating conditions [47]. This has prompted the development of dual-fuel strategies that use a port fuel injection (PFI) system for low cetane number fuels together with a direct Diesel injection system to facilitate ignition. These strategies are compatible with many different combustion modes and can reduce soot emissions and fossil Diesel consumption. A recent review on the use of alcohol fuels in Diesel engines by Vallinayagam et al. showed that interest in such systems has increased dramatically [53]. Another recent study conducted by Verhelst et al. investigated methanol as one of the most promising fuels due to its wide availability and potential to be scaled up in production on a global level from renewable sources [54]. It has been shown that methanol offers important advantages when used in SI engines but can also be used successfully in a CI engine, as shown by Wärtsilä and MAN in their respective medium and small dual-fuel marine or stationary operated engines [23, 44].

2.3.3 Single-fuel mixture direct injection (DI)

The concept of flexible dual-fuel strategy requires the least number of technical changes to an existing system. The idea behind is that a fuel mixture of Diesel and alcohol can, with some modification and additives, been used directly in an CI engine. This has been demonstrated with short chain alcohol fuels, but also with long chain molecules [29, 39]. The advantages are the small amount of changes to be made to an existing system. Studies have shown, however that depending on the alcohol that is used, an exact mixture has to be produced to be chemically stable. Diesel is often not soluble with certain alcohols, which can cause separation problems [14, 22]. In another approach, ethanol was mixed with 5 % ignition improver and a Diesel engine was modified by e.g., increasing the compression ratio (CR) to overcome problems with autoignition. This concept was presented by Scania [49].

2.3.4 PFI and DI

As mentioned earlier, the PFI strategy is widely used in several different LTC combustion regimes, such as HCCI. Recent investigations by Pedrozo et. al showed the potential of reducing NOx and soot and increasing thermal efficiencies, by using ethanol in the PFI and Diesel to ignite the pre-mixture of fuel and air [36, 37]. Another variant of this concept is reactivity controlled compression ignition (RCCI). Port injected alcohol fuel cools the air charge due to evaporation of the fuel and creates a homogeneous mixture. Ignition is then initiated by the direct injection of Diesel until the mixture has reached the reactivity for auto-ignition. It is possible to adjust the fuel reactivity as a function of speed and load. Reitz and Duraisamy identified key advantages of this technology as its ability to comply with soot and NOx emission standards without requiring an additional aftertreatment system, high thermal efficiencies over wide load ranges and greater thermal efficiency than conventional HD Diesel engines. The latter advantage largely stems from a reduction of heat transfer losses. The authors also identified aspects of RCCI requiring further development, such as the need for greater cycle-to-cycle control over the complete load range and the need to adapt aftertreatment systems to cope with relatively low exhaust gas temperatures [40].

2.3.5 Direct Dual-Fuel Combustion

One way to increase the controllability and responsiveness of dual-fuel engines is to directly inject low and high cetane number fuels into the cylinder. Comparatively few studies have examined this strategy, but an early investigation by Ullman and Hare using a HD engine with methanol and Diesel yielded promising results [28, 25, 52]. This approach offers many potential advantages above and beyond low engine out soot and NOx emissions, including greater fuel efficiency and improved engine flexibility. Wissink et al. recently reported a new variant of this strategy using Diesel and gasoline as high and low cetane number fuels, respectively, in an engine operated on the direct dual fuel stratification (DDFS) combustion concept [56, 57]. The concept was described as combining the advantages of RCCI and partially premixed combustion (PPC). However, dual-fuel combustion operating mainly in the diffusion-controlled combustion regime was chosen for the present investigation.

2.3.6 Fuel sprays

Detailed characterization of high pressure alcohol fuel sprays in Diesel-like environments is needed to guide further development of dual-fuel direct injection combustion concepts. Such characterization will facilitate the design of optimized nozzle configurations and also provide important insights into factors affecting the combustion efficiency and engine out emissions. High-speed injection of a fuel jet into the cylinder creates turbulence that promotes spray breakup and vaporization, leading to fuel-air mixing. The local equivalence ratio plays a major role in soot formation, while the efficiency of the mixing process strongly affects the scope for achieving complete combustion and is highly sensitive to the nature of the fuel injection process [48]. The orifice diameter of the injector, in cylinder gas temperature, and ambient gas and fuel densities are the main factors governing spray behavior [4]. Other important factors are properties of the fuel itself, such as its heat of evaporation, boiling point and volatility [46, 5]. One particularly interesting spray property in engine tests is the liquid length, which determines the extent of wetting of the cylinder liner in real engines. It has been shown that the liquid length is only weakly dependent on the injection pressure.

Chapter 3

Experimental Set-up

This chapter presents an overview of the experimental setup and the equipment and procedures used in the experiments. It also describes how the data were post-processed and analyzed. Two experimental setups were used in the course of this project. In the first, a high pressure high temperature (HP/HT) spray chamber was used to characterize the properties and behavior of high pressure ethanol sprays. In the second, the dual-fuel injection strategy was studied at various speed-load points by performing single cylinder engine (SCE) experiments using a Volvo D13 HD engine.

3.1 Fuels and Fueling system

The main fuelling system in both experimental campaigns was a standard Delphi HD common rail fuel injection system operated with methanol, ethanol, E85 and Diesel. The system consisted of an externally driven high pressure pump delivering a maximum pressure of 2200 bar, high pressure pipes, a HD rail for six cylinder truck applications, an F3 or F2 injector and an ECU modified for single cylinder applications. The internal and external rubber seals were replaced to minimize the risk of failure due to the use of alcohol fuels. To avoid cavitation in the return line, which can cause errors when measuring fuel consumption, the system's backpressure was increased to 5 bar. For the engine tests, an additional light duty (LD) Bosch common rail fuel injection system was installed to deliver the pilot Diesel fuel. This system was used exclusively with Diesel fuel, its mode of operation was identical to that of the Delphi system and its ECU was modified for single cylinder operation. Table 3.1 and Table 3.3 present details of all the fuels and injector configurations used in the project to date.

3.2 Spray Chamber Experiments

The HP/HT constant flow spray chamber used in the experiments had an internal volume of 2 l. Its configuration for the spray experiments is depicted in Figure 3.1. Optical access was available through windows on four sides of the chamber;

Table 3.1: Fuel Properties of Diesel, methanol, ethanol and E85.

	Diesel	**Methanol**	**Ethanol**	**E85**	**Unit**
Chemical formula	$C_{10}H_{20}$ to $C_{15}H_{28}$	CH_3OH	C_2H_5OH		
Cetane number	52	5 - 8	<5	n/a	
Lower heating value[a]	42.87	18.95	23.93	27.62	MJ/kg
Density	842	794	792	790	kg/m^3
Heat of Vaporization	~254	~1109	~841	~830	kJ/kg
Carbon[b]	86.2	36.8	48.3	55.7	mass-%
Hydrogen[b]	14.3	12.5	13.0	13.0	mass-%
Oxygen[c]	<0.1	50.7	38.7	31.3	mass-%

Methods used:[a] ASTM D 240, [b] ASTM D 5291,[c] ASTM D 5291 mod.

the windows were around 100 mm long and 50 mm wide. The maximum chamber pressure was 100 bar at temperatures of up to 900 K. These conditions resembled the operating conditions of a HD Diesel engine at low loads [45]. Compressed air was delivered by a four-stage piston compressor and then heated by electrical heaters before entering the vessel. The flow rate of air from the top of the chamber to the bottom was approximately 0.1 m/s, which was negligible compared to the fuel injection velocities of around 200 m/s.

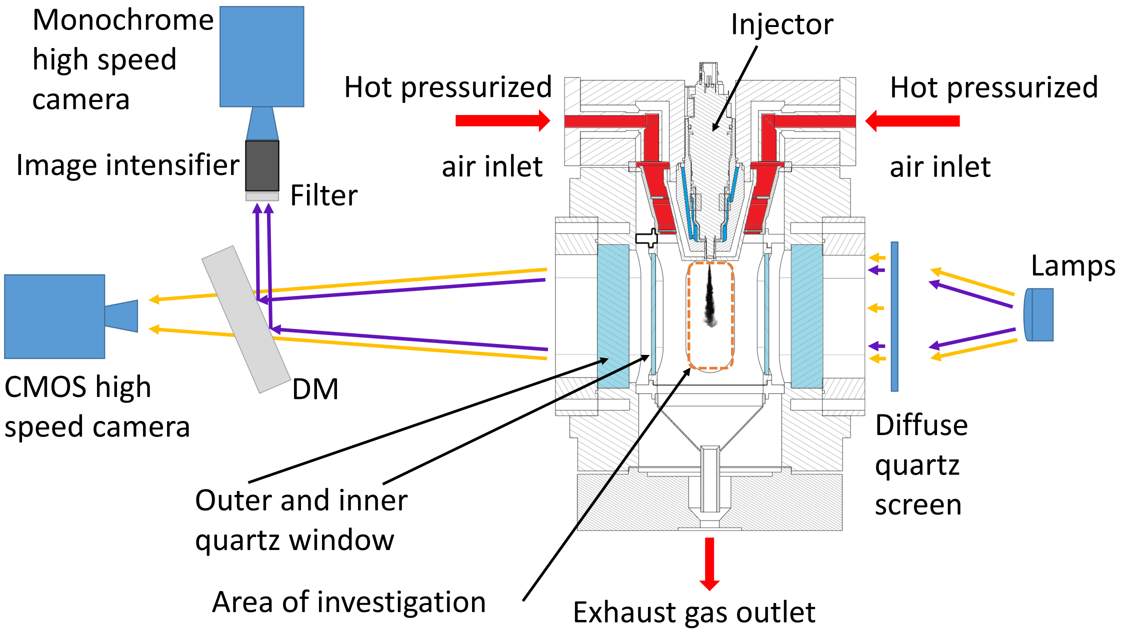
Monochrome high speed camera
Image intensifier
Filter
Hot pressurized air inlet
Injector
Hot pressurized air inlet
Lamps
CMOS high speed camera
DM
Diffuse quartz screen
Outer and inner quartz window
Area of investigation
Exhaust gas outlet

Figure 3.1: Schematic of the spray chamber and optical set-up. Lamps: Two halogen spot lights, one UV lamp at 254 nm wavelength. DM: dichroic mirror (248 nm ± 25 nm). Filter 254 nm. [42]

3.2.1 Optical setup

The sprays were illuminated by two halogen spot lights and one UV lamp with a wavelength of 254 nm, as shown in Figure 3.1. A diffuse quartz screen ensured an even distribution of light intensity. The dichroic mirror on the opposite site of the vessel permitted only the passage of light with wavelengths of 248 nm ± 25 nm, ensuring that the information in the UV light beam was separated from from that in the visible light beam contained in the shadowgraph image. Visible light shadowgraph images were recorded using a high speed CMOS camera with normal optical lenses and provided information on the distribution of the spray's liquid phase. The UV light beam, which provided information on the distribution of the liquid and gaseous phases, was passed through a filter at a wavelength of 254 nm to exclude ambient light and other non-informative light sources before entering an image intensifier. A phosphor screen was installed at the far end of the intensifier, allowing a shadowgraph image to be captured using a monochrome camera. At the desired frame rate of 20 kHz, the resolution of the CMOS and monochrome cameras were set to 256x512 and 480x200 pixels, respectively. The cameras were activated indirectly by the injection pulse and had an exposure time of 10 μs. An additional laser was used to ignite a pilot ethanol spray, which in turn was used to ignite the main ethanol spray. This system was used to simulate Diesel ignition in a real engine and determine whether increasing the dwell time adversely affected the ignition of the main injection. Ignition of the pilot ethanol spray with the laser beam is depicted in Figure 3.2.

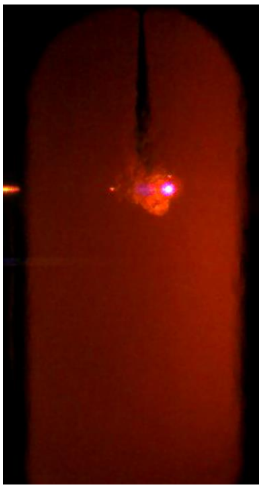

Figure 3.2: Laser ignition test with pure ethanol in the HP/HT chamber at non-autoigniting condtions.

3.2.2 Measurements and spray evaluation

Ten replicate injections were recorded at each measurement point with the same injection duration, pressure and ambient conditions inside the vessel in all replicates. The measurement points examined in the spray experiments are listed in Table 3.2. High speed video recordings were acquired using the monochrome and CMOS cameras together with traces of the injection pulse, the rail pressure, chamber pressure and temperature.

Table 3.2: Experimental conditions used in the spray chamber tests.

Experimental conditions	**Ambient temperature [°C]**	**Ambient pressure [bar]**	**Ambient gas density [kg/m^3]**
Evaporating ethanol spray	550	60	25.4
Evaporating Diesel spray	425	54	27
Evaporating ethanol spray	425	54	27

During post-processing, light intensity thresholds used to extract information from the high speed video images were chosen based on the results reported by Du [8]. The thresholds were adjusted to include diluted droplet clouds, and the spray was assumed to be liquid in regions where the relative light intensity exceeded 0.1 (25/255), obtained by dividing the measured light intensity by the max possible value, here 25 over 255 (where 1 represents the lowest intensity and 255 the highest). The image processing steps is shown in Figure 3.3. This value yielded consistent results for all the tested fuels. The cone angle and liquid and vapor penetration lengths were determined for each individual frame in each video recording, allowing the evolution of the spray over time to be characterized. The liquid penetration length was defined as the distance between the nozzle tip and the most distant liquid fuel droplet along the spray axis. The cone angle (ϕ) was calculated using Equation 3.1, which was developed by Naber and Siebers and yielded reliable results. In this equation, S is the liquid penetration length and A is the "projected spray area of the upstream half of the spray in an image" [30].

$$\frac{\phi}{2} = tan^{-1}\left(\frac{A_{p,S/2}}{\frac{S}{2}^2}\right) \tag{3.1}$$

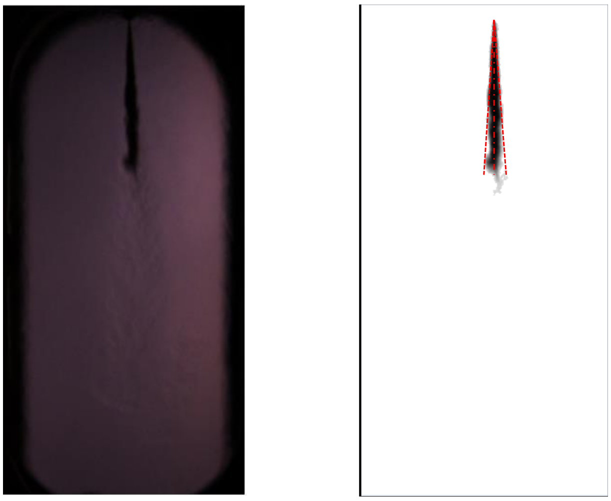

Figure 3.3: The unprocessed image of an ethanol spray on the left and the process grayscale image used during post-processing on the right.

3.3 Engine Experiments

All experiments were performed using a Volvo D13 SCE with the key specifications listed in Table 3.5. Crank angle resolved cylinder pressure traces were recorded in all engine experiments and used to determine a wide range of important combustion parameters by constructing apparent rate of heat release (aRoHR). In combination with fuel consumption and emissions data, parameters such as the combustion phasing, ignition delay, combustion duration, gross indicated efficiency and brake specific emissions were calculated. These data could be used to validate CFD and gas exchange models, enabling optimization of the cylinder head and piston bowl shapes, as well as the positioning and targeting of the fuel sprays from the two injectors. The design of the cylinder head itself was altered (relative to the stock configuration) before the experiments to accommodate two injectors: the main injector (Delphi) was kept in the center of the head and a second (Bosch) injector was mounted alongside it, oriented in such a way that its spray was directed toward the middle of the cylinder.

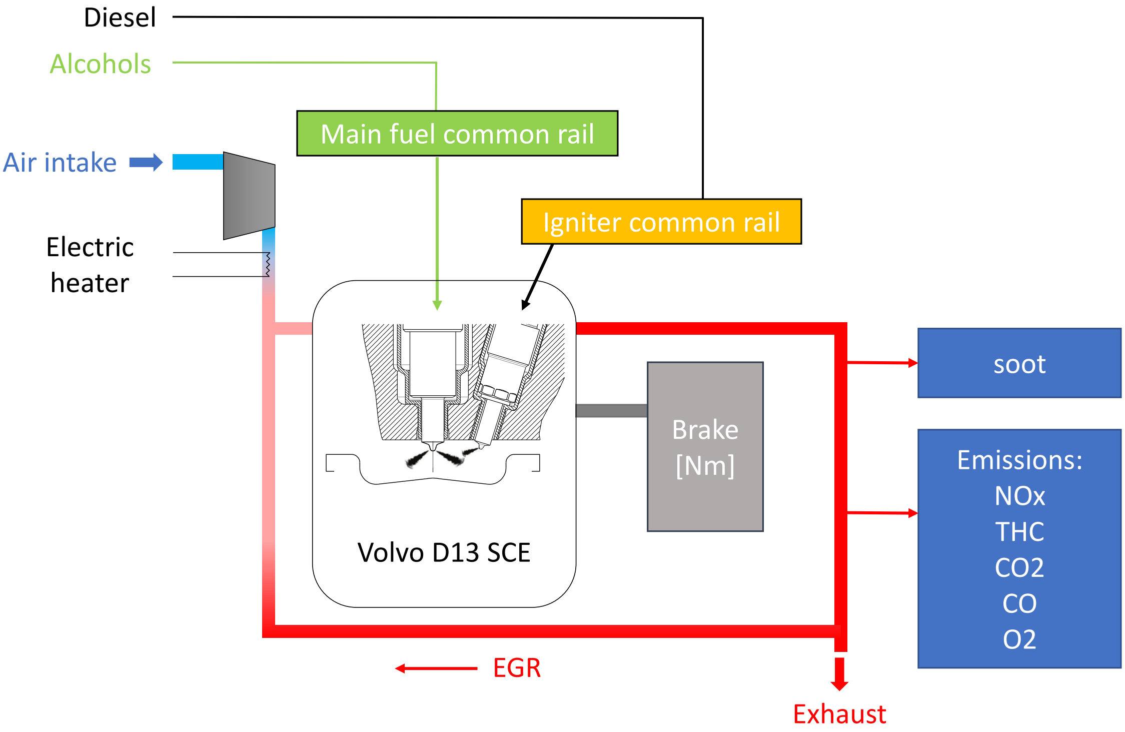

Figure 3.4: Schematics of the SCE test cell setup, including two commonrail systems, exhaust-gas measurement equipment and dual-injector arrangement.

The injector arrangement and adapted standard-piston bowl shape are shown in Figure 3.4. The changes made to a standard ω piston were, lowering the dome of the piston to avoid pilot fuel spray impingement and reducing the diameter of the piston bowl to keep the volume identical and hence the compression ratio (CR) constant at 16.7. Figure 3.5 shows the two pistons used during the course of the experimental tests, with Figure 3.5a showing the adapted standard-piston and Figure 3.5b showing

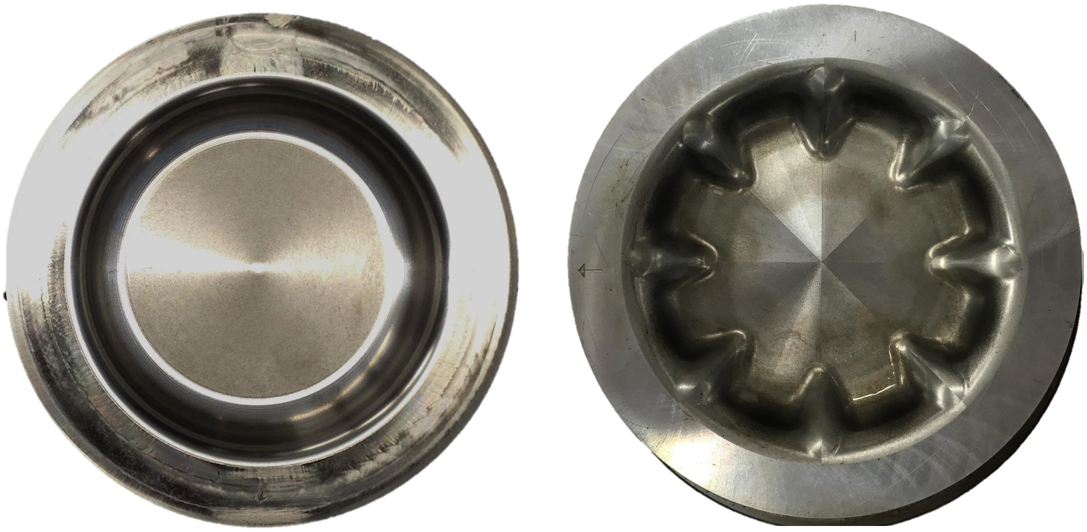

(a) FFlex standard-piston used during the experiments.

(b) FFlex wave-piston used during the experiments.

Figure 3.5: Both piston types used were adapted from the standard ω piston and standard wave-piston.

the adapted wave-piston. The standard wave-piston has 6 or 7 waves, depending on the Diesel injector used. Here the adapted wave-piston has 8 waves, the same number as the fuel injector has nozzle holes. Figure 3.6 shows the setup in the test cell with two commonrail systems installed. Five different speed-load points were studied to evaluate the combustion behavior of the methanol-Diesel dual-fuel system, as shown in Table 3.4. Each of these points was related to the corresponding speed-load points for a Volvo D13 six cylinder engine with 460 horsepower and a maximum torque of 2346 Nm by dividing the multi-cylinder load by 6 and then applying an additional loss factor of around 4 %. The 1262 rpm and 172 Nm point was of most interest because it corresponded roughly to the conditions at a truck's cruising speed, and thus the most common operating state of the studied HD Diesel engine.

Table 3.3: Specifications of injectors used throughout the test campaigns.

Engine Tests	**Name**	**Details**
Bosch (side)	CRI2-18	3-hole, asymmetric
Delphi (alcohols)	F3 (DFI5)	8-hole, 4.65 l/min at 100 bar, 147°
Delphi (Diesel)	F2 (DFI21)	6-hole, 2.3 l/min at 100 bar, 150°
Delphi (alcohols)	F3 (DFI5)	7-hole, 3.0 l/min at 100 bar, 145°
Spray Chamber Tests		
Delphi (Diesel)	F2 (DFI21)	single-hole, 0.34 mm orifice diameter
Delphi (Ethanol)	F3 (DFI5)	single-hole, 0.32 mm orifice diameter

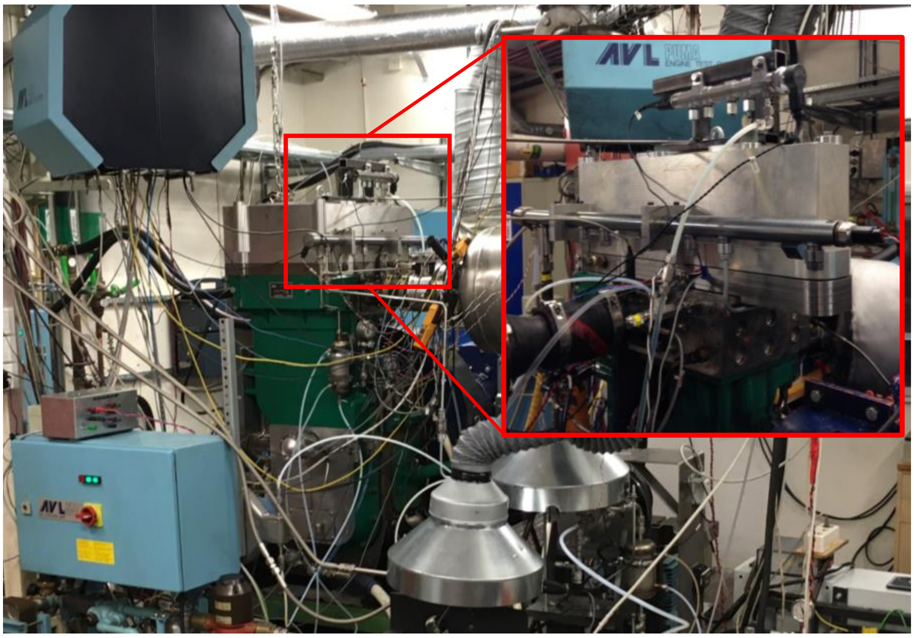

Figure 3.6: Picture of the SCE test cell setup, including the two commonrail systems for the dual-injector setup.

Table 3.4: Speed-load points investigated.

Point description	Speed [rpm]	Torque [Nm]
Low speed, low torque	871	86
Medium speed, medium torque	1262	172
High speed, high torque	1508	285
Rig stability check	1400	305

3.3.1 Data acquisition and handling

Figure 3.4 depicts the experimental setup used in the test campaigns. An AVL Puma Open system controlled the electric dynamometer (and hence engine speed) and measured the engine's torque. The Puma system was connected to two AVL 733S/753C fuel conditioning systems that measured fuel consumption and also regulated the temperature and pressure of the fuel entering the high pressure pumps. A plenum at the intake and exhaust manifolds stabilized the air and exhaust gas flows and reduced pressure fluctuations into the engine and downstream toward the exhaust gas emission measurement equipment. The intake and exhaust pressures were also regulated by the Puma system via sets of valves located before the inlet of the plenum and after the exhaust plenum to ensure constant inlet and outlet pressures.

An AVL AMA i60 R1C-EGR exhaust measurement system was used to perform sampling downstream of a back-pressure valve in the exhaust system through a heated pipe. Soot emissions were measured with an AVL 483 micro soot sensor at the same point. On every test day, before and after measurements at each new

Table 3.5: Volvo D13 HD single cylinder research engine specifications.

	Value	**Unit**
Displacement	2.1295	dm^3
Bore	131	mm
Stroke	158	mm
Valves	4	
Compression ratio	16.7:1	
Inlet valve closing (IVC)	138.5	°bTDC
Exhaust valve vpening (EVO)	130	°aTDC
Maximum cylinder pressure	200	bar
Maximum pressure rise rate	20	bar/CAD
Swirl number	0	

speed-load point, a rig stability check (RSC) was executed at the high speed-load point of 1400 rpm and around 305 Nm. The mean measured emissions and their errors at this load point were calculated each time, giving an indication of the tests' repeatability. The volume flow of intake air was calculated based on the measured CO_2 levels in the intake and exhaust. All data were recorded for 2 minutes by the Puma system and saved as averaged values over that time frame. The HD and LD fuel injection systems were controlled using ATI Vision from a separate computer. The injection pressure, timing and duration were set directly based on the test point being investigated. The high pressure pumps were driven by external electrical motors at a constant speed.

An Osiris fast data acquisition system was used for high frequency recording of the cylinder pressure and cylinder volume, the injector current pulses of both injectors and the intake temperature and pressure before the intake valve. All these variables were resolved in crank angle degrees (CAD) at a resolution of 0.1 deg. The pressure was measured with an AVL QC34C pressure transducer with a measurement range of 0 to 250 bar. The position of the peak pressure during a motored case was recorded before every run and adjusted to 0.6 deg before top dead center (°bTDC), which was determined to be the thermodynamic loss angle for the studied engine based on measurements. One hundred complete four-stroke engine cycles were recorded at each measurement point.

3.3.2 Methods

The measured data were evaluated and post-processed using a Matlab code written in-house. An important variable for describing the quality of combustion is the gross indicated fuel efficiency, $\eta_{f,ig}$, which was calculated from the gross indicated work per cycle as described by Heywood [17]. Therefore, only the compression and expansion strokes were included in the calculations. The pressure signal p was filtered using a Savitsky-Golay filter with a window length of 9 CA and a polynomial fit of the 4th order.

The aRoHR was calculated to obtain the heat release (HR) for each fuel. No modeling of heat transfer to the combustion chamber walls (piston, cylinder head, and liner) was attempted, but the aRoHR calculations provided valuable information about differences between alcohol-Diesel and pure Diesel with respect to variables such as the combustion timing, aRoHR and combustion pattern for given levels of $\eta_{f,ig}$ when using similar injection strategies [17]. The derivation of the heat release is well explained in Heywood and results to equation 3.2:

$$\frac{dQ}{dCAD} = \frac{\gamma}{\gamma - 1} p \frac{dV}{dCAD} + \frac{1}{\gamma - 1} V \frac{dp}{dCAD} \tag{3.2}$$

The equation is in the crank angle domain with Q as the apparent heat released, p as the pressure, V as the volume and γ as the ratio of specific heats. The specific heats were calculated at each time step during the combustion process, due to their temperature dependency. This was done in accordance to the polynomials and tables published by the American National Institute of Standards and Technology [24].

A design of experiment (DoE) study was used to maximize the amount of information gained from the limited number of experiments that could be performed [41]. The design was performed using the MODDE Pro 12 software package from MKS Umetrics AB [43]. The measurements were optimized using a Central Composite Face (CCF) design based on a full or fractional factorial design with a full quadratic model including all two-factor interactions and all square terms of all factors. The terms represent the factors, the factors squared, the factors multiplied with each other and a multiplication of the squared terms and are used to calculate the regression model. This is resulting in a surface response plot filling the missing information between the points measured.

Chapter 4

Summary of Publications

This chapter gives a brief overview of already published results. The first paper describes a spray investigation of high pressure ethanol injection compared with Diesel. The second paper compares and discusses dual-fuel SCE tests with methanol-Diesel and Diesel as a reference. The third paper describes how the experimental setup was used to investigate the auto-ignition properties of methanol or ethanol blended with 5 % polyethylene glycol as an ignition improver in order to test additional options as a reference to the dual-fuel tests. In the fourth paper, a comprehensive analysis of methanol, ethanol and Diesel dual-fuel tests on the SCE at three different speed-load points is presented.

4.1 Paper I

"High Pressure Ethanol Injection under Diesel-like Conditions"

Paper I describes studies on the evolution of ethanol fuel sprays over time. The sprays were characterized in terms of their liquid and vapor penetration lengths and liquid spray cone angle, and were compared to Diesel fuel sprays generated under the same conditions. The experiments were performed at a gas density of 27 kg/m^3 at 550 °C and 60 bar, representing typical operating conditions for a HD engine at low loads. In addition to providing valuable data on alcohol spray properties, these studies served as a successful proof of concept demonstrating that a Diesel common rail system can be used with an alcohol fuel at injection pressures up to 2200 bar. The injection pressure was confirmed to have only a minor effect on the liquid penetration length, and there was a strong correlation between the gas temperature and liquid penetration length for ethanol sprays. Ethanol sprays were also shown to have shorter liquid lengths than diesel sprays under the same engine operating conditions.

4.2 Paper II

"Dual Fuel Methanol and Diesel Direct Injection HD Single Cylinder Engine Tests"

Paper II can be viewed as a continuation of the proof of concept under real engine conditions, this time using methanol. It was shown that a standard high pressure Diesel injection system can be employed without significant problems in an SCE using a methanol-Diesel dual injection combustion strategy. The combustion properties of the dual-fuel system were compared to those of pure Diesel with the same dual injection strategy. The methanol-Diesel system exhibited stable and controllable combustion at the tested speed-load point. Moreover, the methanol system achieved a similar fuel efficiency to conventional Diesel, with lower NOx emissions and significantly lower soot emissions. However, it also yielded higher peak cylinder pressures and peak pressure rise rates. In addition, a DoE study showed that a good predictive regression model could be developed for the methanol-Diesel system based on a small number of experiments, greatly increasing the scope for interpreting the system's behavior.

4.3 Paper III

"CI Methanol and Ethanol Combustion Using Ignition Improver"

Paper III can be seen as an excursion from the original concept toward a single-fuel approach. During this investigation, methanol and ethanol were blended with an ignition improver to increase the cetane number. 5 % polyethylene glycol was added and tests were conducted at the standard CR of 16.7 and an increased CR of 20. A partially premixed CI regime was achieved by using a pilot-main injection strategy. All tests were performed at medium speed-load conditions of 1262 rpm and 172 Nm. The higher CR performed significantly better in terms of $\eta_{f,ig}$, NOx emissions and lower combustion noise. Nevertheless, the control of the combustion event and physical limitations due to peak pressure rise rates and peak cylinder pressure, compared with the initially investigated dual-fuel engine, made the single fuel option less favourable.

4.4 Paper IV

"Alcohol flexible HD Single Cylinder Diesel Engine Tests with Separate Dual High Pressure Direct Fuel Injection"

Paper IV can be seen as a comprehensive continuation of Paper II. SCE tests were performed at low, medium and high speed-load conditions. Additionally, EGR was used to further reduce thermal NOx formation. It was shown that methanol and ethanol always outperformed Diesel in the flex fuel engine setup and under all speed-load conditions tested when investigating the $\eta_{f,ig}$, ISNOx, ISSOOT, ISCO2 and when using EGR. The fuel substitution ratio was over 95 % and the combustion stability was not compromised in any way.

4.5 Paper V

"CFD Modeling of a Direct Injection Dual Fuel Engine"

In this paper a CFD model has been constructed and tested for a direct-injection dual-fuel engine that uses low carbon alcohol fuels, such as methanol, ignited by a pilot injection of Diesel. A tabulated version of the Well-Stirred Reactor (WSR) approach called CPV was evaluated. The simulations showed good agreement when comparing the pressure and rate of heat release curves with experiments. Furthermore, the ignition process was investigated in detail and it shows a very short ignition delay with nearly no premixed phase due to the methanol being injected in close proximity to the hot gases from the Diesel pilot. The prediction of emissions was also investigated, which showed a very good agreement for CO_2, and an over-prediction by a factor of 2 for NO_X emissions, which is consistent with the tabulated well stirred reactor (WSR) approach used in this work.

Chapter 5

Results and Discussions

This thesis consists of results from four papers appended to this thesis and represent the main results from the test campaigns throughout the course of this project. However, some investigations have not been published and the most interesting of those results are presented in this chapter. Firstly, a detailed investigation into the stability and repeatability of the experimental setup is described, followed by a comprehensive DoE investigation. This included a comparison of results for three alcohol-based fuels, i.e., methanol, ethanol and E85, with those for Diesel. This evaluation was followed by a short analysis of the influence of the wave piston on the dual-fuel combustion. Furthermore, investigation into the influence of the hydraulic flow of the injector on the dual-fuel combustion and its emissions was conducted.

5.1 Rig Stability Check (RSC)

This section describes how RSC data were collected and used to provide an insight into the repeatability and stability of the measurement results. Table 5.1 presents the main settings during each reference measurement for the separate fuels. These measurements were repeated during every test day. All measurements were made under similar initial conditions and with identical hardware, except for the lower flow number nozzle for Diesel. A small error is vital for a comprehensive investigation. Thus, error bars were used to represent the repeatability of a certain result for a given fuel, calculated as the standard deviation of the repeated RSC. Error bars are also shown in the results plots for the respective fuels.

Table 5.1: Summary of the settings for the different fuels at RSC at 1400 rpm and 305 Nm, P_{main} as the pressure of the main injection, and SOI_{main} as the start of the injection event of the main injection.

Fuel	$\mathbf{P}_{main}$ **[bar]**	$\mathbf{SOI}_{main}$ **[°bTDC]**	$\mathbf{Duration}_{main}$ **[ms]**
Diesel	1250	6	1.990
Methanol	1250	4	1.990
Ethanol	1250	3.5	1.565
E85	1250	3.5	1.380

Figure 5.1 shows two plots of calculated and measured results, including error bars for both axes. Figure 5.1a presents the $\eta_{f,ig}$ vs. ISNOx emissions and shows two key results used to evaluate the flex fuel engine for the respective fuels. The thermal efficiency was obtained from high frequency in-cylinder pressure recordings as well as 2 min averaged fuel consumption measurements. At least nine RSC measurements from nine different test days are included in this plot. The small spread of the data points suggests that the relative error was small, in this case well below 1 %. The error for ISNOx was also generally small and only calculated from data with low sampling rate, collected and averaged over 2 min. Even though the errors were generally small, a few distinctions for the different fuels can be pointed out. Firstly, Diesel had the smallest errors, which can be attributed to the components used during the experimental campaigns. Besides the larger flow number nozzle, none of the engine components were specifically designed for low viscosity fuels. Only the PID control parameters on the HD common rail pump system, for adjusting the response of the opening and closing of the release valve at the rail and the metering valve at the pump side, were modified to cope with the alcohol fuel properties, such as viscosity.

Figure 5.1b shows the errors of the fuel measurements, which were very small for the main fuel but not so small for the pilot fuel. The fuel quantity used on the pilot side was too small for a HD dimensioned fuel balance. Nevertheless, large errors were only observed when using ethanol as the main fuel but were not significant enough to cause problems with the measurements. At no time was there any problem with the ignition process of the alcohol fuels during tests without EGR. This indicates that the larger fluctuations of the pilot Diesel amount did not cause any instabilities during the ignition process.

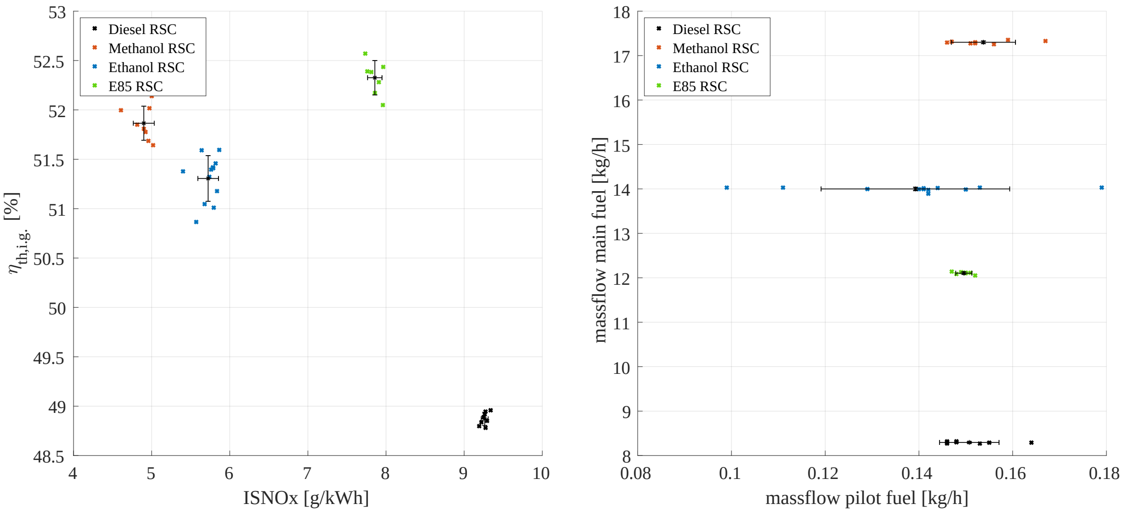

(a) Indicated thermal efficiency vs. ISNOx in the RSC, including error bars.

(b) Fuel consumption of the main fuel and pilot fuel in the RSC, including error bars.

Figure 5.1: Plots of measurement errors from the RSC.

Since three speed-load cases were investigated in depth, all conditions in the RSC were examined are complementary. Figure 5.2a shows aRoHR curves for all the RSC points plotted in Figure 5.1. The aRoHR curves of ethanol and E85 were very similar, with a slightly higher and earlier peak for E85 than for ethanol. The gradient of the aRoHR for the alcohol fuels was generally steeper during the initial combustion phase, suggesting faster combustion during the free-flame phase. All HR gradients decreased after the combusting flames hit the cylinder wall and flame-wall interactions slowed down the combustion. The curve for methanol peaked slightly higher than that of Diesel but significantly lower than for the ethanol fuels. This can be ascribed to the higher LHV of the ethanol fuels for the same injection pressure and nozzle configuration. These findings are in accordance with results for the high speed-load case presented in Paper IV. The spider plot of the main results in Figure 5.2b shows that the three alcohol fuels outperformed Diesel in terms of the $\eta_{f,ig}$, ISNOx and ISCO$_2$, whereas Diesel performed slightly better for ISCO and ISHC. The combustion duration was significantly longer for Diesel, as evident by the more pronounced tail for Diesel compared with methanol combustion in the HR curves. Ethanol and E85 are closer to methanol.

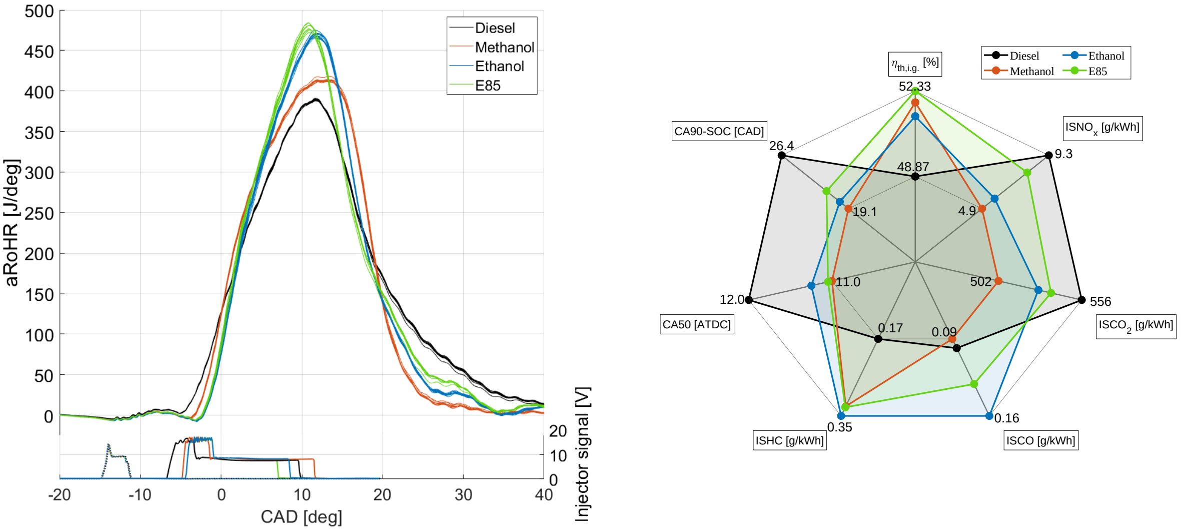

(a) aRoHR curves for all RSC conditions investigated.

(b) Spider plot for all RSC conditions investigated.

Figure 5.2: aRoHR curves, emissions, engine, and combustion data for methanol, ethanol, E85 and Diesel in the RSC.

In summary, the repeatability of the measurements was found to be within a reasonable range and error bars for the various results were based on the first standard deviation from the mean of the RSCs conducted for each fuel. The results of the RSCs for the different fuels were in line with previous investigations presented in papers II and IV.

5.2 Design of Experiments

In this section, a general overview is provided of the DoEs for methanol, ethanol and E85 compared with that for pure Diesel. A good approach is to use a central composite face design consisting of a full or fractional design, as presented in Paper II. Relevant factors are presented in Table 5.2. The main limitations were the maximum cylinder pressure of 200 bar and late end of injection (EOI) to reduce the possibility of alcohol fuel spray impinging on the cylinder liner, and thereby removing the lubrication oil. A multiple linear regression model was fitted to the results and included factors, interactions, squares and, for cases with more than two factors, also interaction squares. The procedures for deriving response plots and adding or removing condition terms are well described in Paper II.

Table 5.2: Factors used for for most DoEs (may vary, e.g., due to limitations).

Factor		**Limitations**
P_{main}	500 to 2000 bar	$P_{peak,cyl}$, late SOI $_{main}$
SOI	12 to 0 °BTDC	$P_{peak,cyl}$, late SOI $_{main}$

5.2.1 1262 rpm 172 Nm

This subsection summarizes the DoE results for the four fuels investigated at a speed of 1262 rpm and load of 172 Nm. Figure 5.4 and Figure 5.5 show the response plots of indicated thermal efficiency, combustion duration (DUR), indicated specific NOx emissions and peak cylinder pressure for each fuel from top to bottom respectively. The SOI was varied from 12 °bTDC to TDC and is plotted on the x-axis, whereas the injection pressure is plotted on the y-axis.

The indicated thermal efficiency response plots of the four fuels are presented in the first row of Figures 5.4 and 5.5, with a peak value of about 47 % for Diesel. It covers a large portion of the area investigated and shows that a higher injection pressure is favorable. These results are as expected for a Diesel combustion DoE because increased injection pressure increases the turbulence induced by the fuel jet injected into the cylinder, thereby significantly improving the fuel-air mixing process. The response plot of the combustion duration for Diesel in the second row of Figure 5.4 supports this hypothesis as it shows the shortest combustion duration at a high injection pressure for a late and close to TDC SOI. The local maximum of the indicated thermal efficiency for methanol was about 50.5 %, outperforming Diesel significantly. This result is in line with results presented in Papers II and IV and other research publications [ref]. Ethanol and E85 also outperformed Diesel, with local peaks at around 50 % indicated thermal efficiency (top row of Figure 5.5). The alcohol fuels' lowest efficiencies were better than the highest for Diesel combustion. The peak efficiencies for Diesel and E85 appeared to be a global maximum, whereas the peaks for methanol and ethanol appeared to be only local, with the global maximum potentially lying outside of the investigated area. The results showed that the highest efficiencies were at or close to the corner points of the investigated area, at either high injection pressure and late injection or low injection pressure and early injection. This was also reflected in the response plots of the indicated specific CO_2 emissions (Row I of Figure 5.3). This implies that the regression model did not distort the view of the results and could be considered a good mapping of the results, especially in combination with high R2 and Q2 values at a 95 % confidence level.

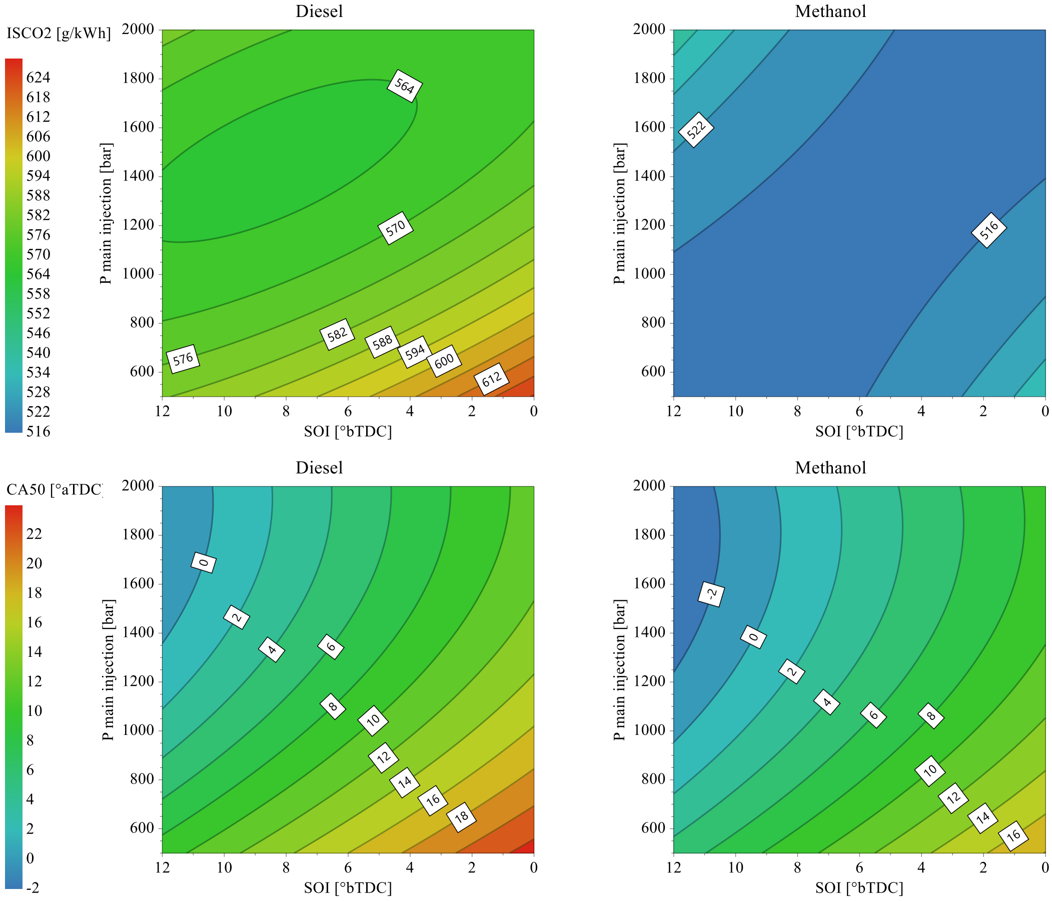

Figure 5.3: Response plots of Diesel and methanol; Row I: $ISCO_2$; Row II: CA50.

The second row plots in Figures 5.4 and 5.5 show that the combustion duration for the three alcohol based fuels, which were all significantly shorter than that for Diesel. Methanol and ethanol had the shortest combustion duration of about 13.5 CAD, followed by E85 at about 15 CAD. As for Diesel, the shortest combustion duration was always in the region of high injection pressure and close to TDC main injection timings. For methanol, reducing the injection pressure appeared to have a smaller effect on increasing the combustion duration than for the other fuels. This indicates that the oxygenation level of a fuel may have an additional effect on the combustion speed and duration. The turbulence induced by injecting the liquid fuel was reduced with a lower injection pressure, and in turn fuel-air mixing became worse fairly equally for all fuels. Methanol showed the least decrease in combustion speed and/or combustion duration, which may partially be explained by it having the largest proportion of oxygen of the four fuels tested.

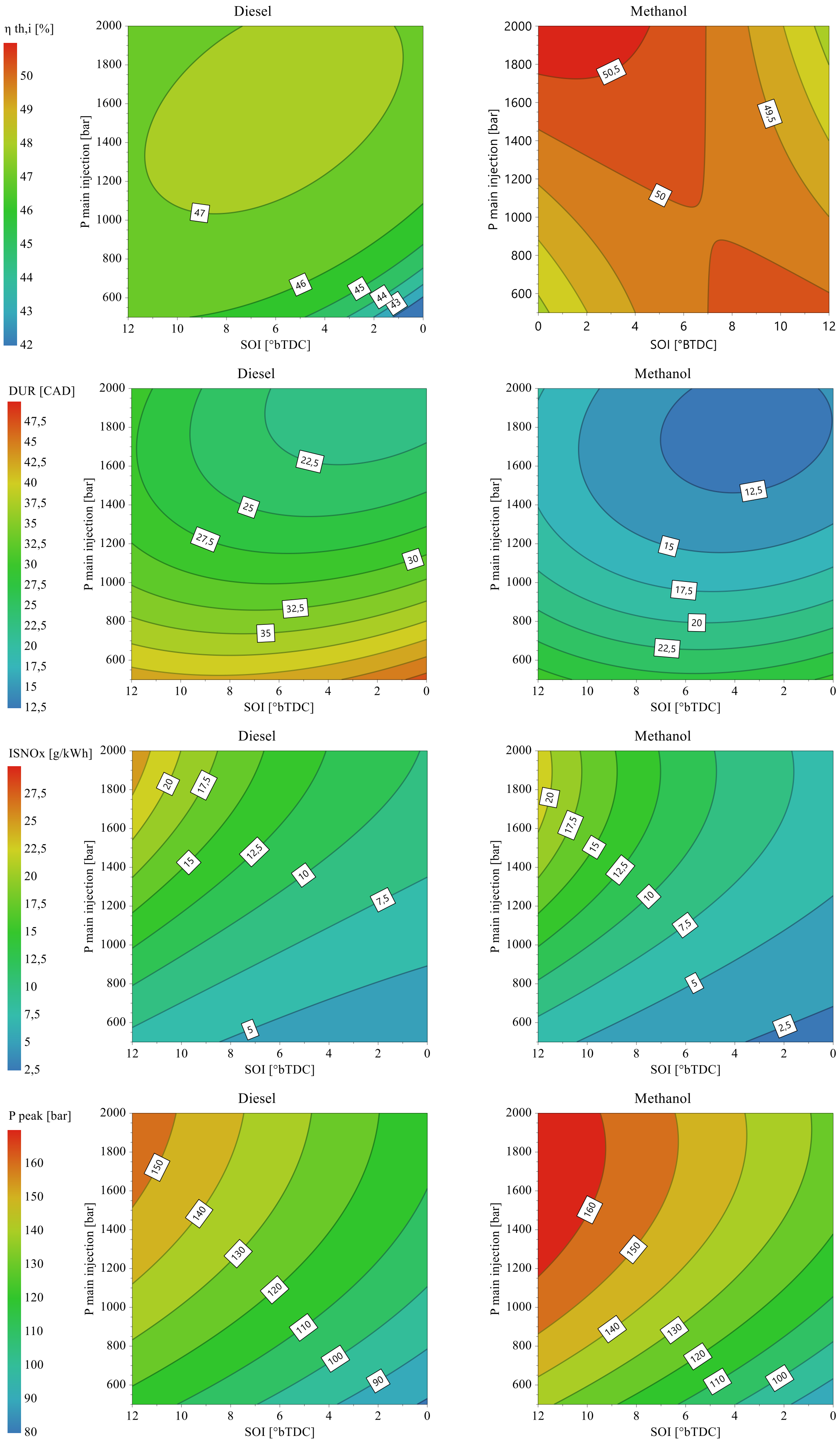

Figure 5.4: DoE response plots for Diesel and methanol Row I: indicated thermal efficiency; Row II: combustion duration; Row III: ISNOx; Row IV: peak cylinder pressure.

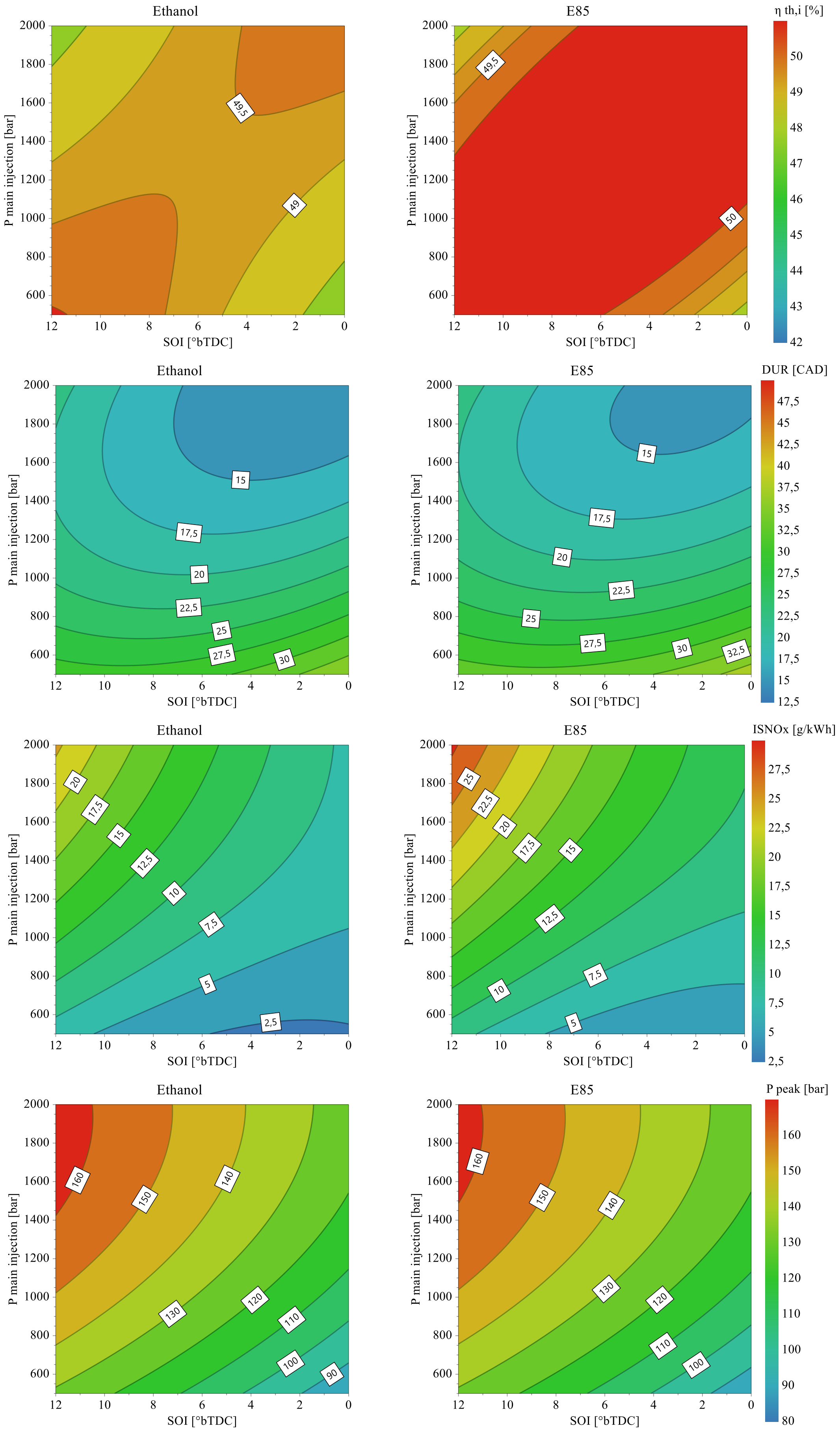

Figure 5.5: DoE response plots for ethanol and E85 Row I: indicated thermal efficiency; Row II: combustion duration; Row III: ISNOx; Row IV: peak cylinder pressure.

The third row response plots of Figures 5.4 and 5.5 show the indicated specific NOx (ISNOx) emissions. The results were very similar for all fuels. The highest ISNOx emissions occurred for an early SOI and high injection pressure, resulting in most of the combustion taking place around TDC. This leads to high temperatures and pressures, which support thermal NOx formation. This was also reflected in the response plot for peak pressure, which showed a maximum in the same region as for ISNOx (fourth row of the figures). It was noticeable that the surface area for high ISNOx emissions was larger for Diesel and E85 than for methanol and ethanol, even though the peak cylinder pressure was higher for methanol. This may be due to differences in the heat of vaporization and amount of liquid injected. Methanol has the highest heat of vaporization, followed by ethanol, E85 and Diesel. The cooling effect of the fuel was one factor, but it was also evident that the LHV was significantly lower for methanol. In return, more fuel mass had to be injected, cooling the ambient air in the cylinder at the SOI even further, creating a better environment to avoid thermal NOx formation. Soot emissions have been reported to be extremely low for the alcohol fuels, as confirmed during the course of the DoE investigation. Therefore, no additional plot is shown here.

Two measurement points of the DoE were selected to compare the four fuels in more detail by plotting their aRoHR and main emissions and other important results. The first point of interest was the center point of the DoE, which was repeated four times each (marked by a red dot in Figure 5.4). This point was chosen because it gave good thermal efficiency results for all fuels. The injection pressure of the main fuel was set to 1250 bar at an injection timing of the main fuel of 6 °bTDC. In an earlier investigation (presented in Paper IV), the aRoHR of methanol, ethanol and Diesel were compared based on a similar combustion phasing. In this case, CA50 was recorded as a response.

Figure 5.6 shows aRoHR curves for the four fuels at 1262 rpm and 172 Nm. In Phase 1 and 2, the HR from the pilot Diesel was followed by ignition of the main fuel. The ignition delay was longest for Diesel and shortest for methanol, whereas the values for E85 and ethanol were very similar, with a slightly longer delay for the latter. A premixed combustion phase was not detected. Thus, the ignition was followed by a free flame combustion phase with diffusion burn, which was significantly faster for the alcohol fuels. The combustion speed was also greater for the ethanol fuels than for methanol. This is likely because of the higher LHV of ethanol since all the fuels were injected at the same injection pressure, causing a higher energy injected per CAD compared to methanol. This phenomenon was also reflected by a slightly steeper HR curve and shorter injection duration, apparent from the shorter injector current signal. Around TDC, the combustion speed slowed down slightly, indicating that the combusting main fuels had hit the piston bowl. This phase (III) was more pronounced for the Diesel fuel. Phase IV started close to the peak of the HR curves, where flame-flame interaction between adjacent sprays was prominent. The alcohol curves peaked slightly above 350 J/deg and Diesel significantly lower and later at about 300 J/deg. E85 peaked first and showed the highest indicated

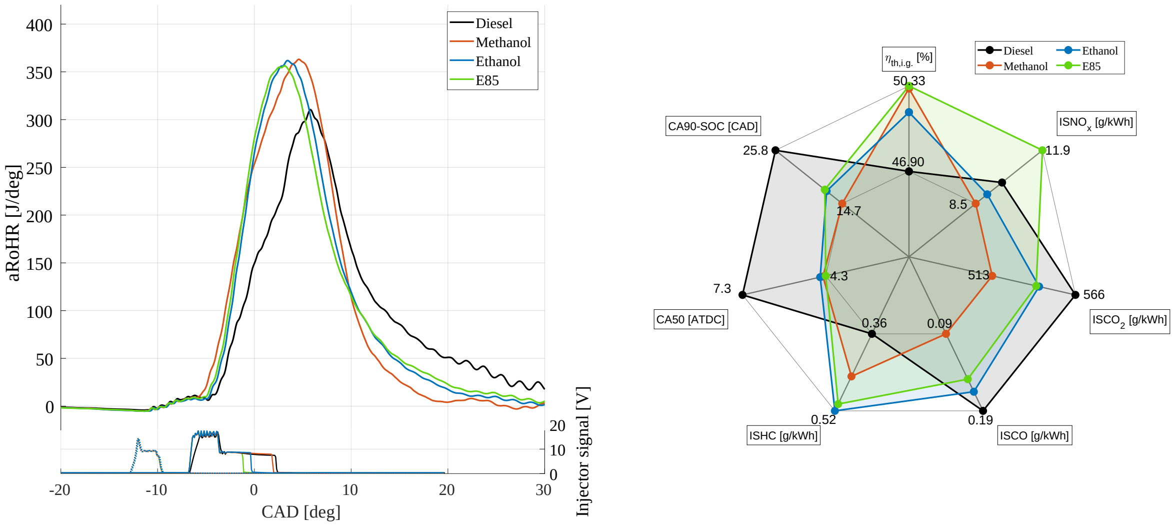

(a) aRoHR curves.

(b) Spider plot of the most important results.

Figure 5.6: aRoHR curves, emissions, engine, and combustion data for methanol, ethanol, E85 and Diesel at 1262 rpm, 172 Nm, 1250 bar injection pressure and SOI at 6 °bTDC.

thermal efficiency but also highest ISNOx emissions, as shown in the spider plot of Figure 5.6b. This indicates that the combustion temperatures were potentially higher for E85, and therefore supported thermal NOx formation, resulting in the highest ISNOx emissions of all the fuels. Following the decrease in the HR curves, the tails are important, corresponding to late cycle oxidation. The methanol tail was by far the shortest, followed by very similar tails for the ethanol fuels, and then a fairly long tail for Diesel. This was reflected in the soot emissions, which were significantly lower for the alcohols.

The spider plot in Figure 5.6b directly compares various results of the fuels. The alcohol fuels all outperformed Diesel in the $\eta_{f,ig}$ by at least 3 % but also in ISCO$_2$ and ISCO emissions. This was mainly due to the different carbon content of the fuels (lowest for methanol). Diesel performed slightly better for ISHC emissions. Interestingly, the CA50 for Diesel was much closer to the engine's nominal thermodynamically favorable point of around 7 °aTDC, compared to the alcohols CA50 of around 4.3 °aTDC. This may be explained by the combustion duration, which was about 10 CAD faster for methanol than for Diesel.

The second point of interest was at an injection pressure of the main fuel of 500 bar and 12 CAD BTDC injection timing (Figure 5.7). The indicated thermal efficiencies for methanol and ethanol seem to have a local maximum at this point in the response plots (Figures 5.4 and 5.5), whereas E85 and Diesel had an absolute maximum at higher injection pressure closer to the TDC injection timing area.

In contrast to the DoE center point described above, the different phases of combustion were more pronounced, as shown in Figure 5.7a. This was due to the

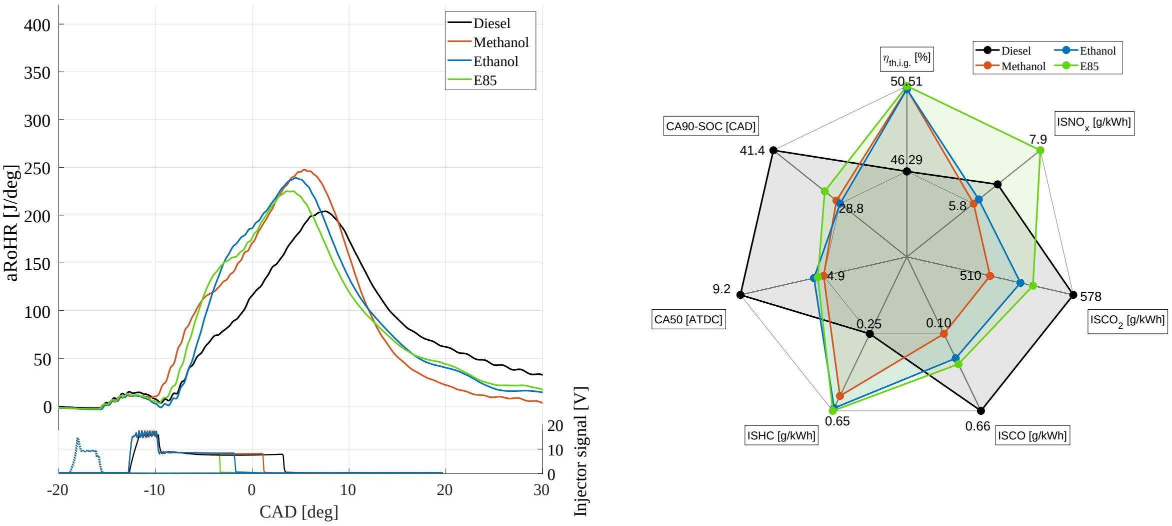

(a) aRoHR curves. (b) Spider plot of the most important results.

Figure 5.7: aRoHR curves, emissions, engine data, and combustion data for methanol, ethanol, E85 and Diesel at 1262 rpm, 172 Nm, 500 bar injection pressure and SOI at 12 °bTDC.

lower injection pressure, and therefore slower combustion, at the same engine speed of 1262 rpm. At the end of Phase I, after combustion of the Diesel pilot, in contrast to the previous case, the ignition delay of ethanol was slightly longer than for Diesel. However, methanol and E85 retained a significantly shorter ignition delay. A possible explanation could be differences in evaporation temperature, represented by a low boiling temperature. Methanol has the lowest (at 64.7 °C) followed by ethanol (at 78.2 °C) and Diesel (from 180 to 360 °C). E85 contains a significant amount of gasoline (boiling range from 30 to 210 °C), supporting the evaporation of E85 at a lower temperature. After start of combustion (SOC) of the main fuels, the alcohol fuels showed a significantly greater increase in the HR rate, which in return suggests faster combustion during the free-flame combustion of Phase II. The start of combustion, Phase III, i.e., the flame-wall interaction phase, was clearly visible for all the fuels at the point where the HR curves slowed down significantly for the first time after SOC. Phase IV began just before the aRoHR curve peaked, with methanol having the highest peak of nearly 250 J/deg, followed by ethanol and E85. Diesel peaked later than the three alcohols at about 200 J/deg. The behavior after the EOI was similar to that described before. Methanol exhibited a very short tail, whereas ethanol and E85 had a slightly longer tail and Diesel had the most pronounced one.

Figure 5.7b summarizes the main results evaluated at the chosen settings. The indicated thermal efficiency ($\eta_{f,ig}$) was very similar for all three alcohol fuels and about 4 % higher than that of Diesel. At the same time, ISNOx emissions were lower for methanol and ethanol (just under 6 g/kWh) and larger for E85 (7.9 g/kWh). This indicates higher combustion temperatures for E85. These values are generally lower compared with the values presented in Figure 5.6b. The higher injection pressure improved fuel-air mixing due to increased turbulence, and thus increased the speed of combustion. Additionally, more fuel per CAD, and therefore more energy, was injected per time unit, increasing the combustion temperature in the cylinder during the combustion. The other emission values were similar to the previous case, with CO_2 being significantly lower for methanol than Diesel, and ethanol and E85 having values in between. The combustion duration was significantly increased due to the lower amount of energy injected per CAD. Diesel had a considerably longer combustion duration than the alcohol fuels. The combustion phasing was retarded for all cases, but the distance between CA50 of the alcohol fuels and Diesel increased. This shows that the enhanced air-fuel mixing process due to a higher injection pressure had a greater impact on Diesel than on the alcohol based fuels. This can be attributed to the oxygen already available in the alcohols.

5.2.2 1262 rpm 172 Nm EGR

In this section, DoE results of tests performed with EGR are presented. Previous investigations have shown that especially methanol generates lower ISNOx emissions compared to Diesel. EGR was added as a third factor to reduce those emissions even further. The injection pressure range was reduced to 500 to 1500 bar and EGR was varied from 0 to 30 %. The back pressure on the exhaust side was increased by 200 mbar to drive the EGR system. No EGR-cooler was mounted on the system. Additionally, a wave piston was used to study the effects of a state-of-the-art piston shape on methanol-Diesel dual-fuel combustion. The wave piston was used to enhance mixing of Diesel and air, especially during the latter part of combustion, reducing soot emissions. It has been extensively studied by Eismark [10, 9] and will be described in more detail in the following sub-chapter. Figure 5.8 for three cases at 15 % EGR: Diesel as a reference is on the left hand side, methanol with a standard piston in the middle and methanol with a wave piston is on the right. The injection pressure is represented on the y-axis, whereas the SOI of the main fuel is on the x-axis from 12 °bTDC to TDC.

Under EGR conditions, the methanol results consistently outperformed Diesel in terms of $\eta_{f,ig}$ over the whole range investigated. All three sets of results showed the lowest efficiency at low injection pressure (500 bar) and late injection timing, which correlates to a later and longer combustion duration. However, ISNOx emissions were the lowest in the same region. This is because the main part of the combustion took place long after TDC during the expansion stroke at fairly low combustion temperatures. The low injection pressure could not deliver sufficiently fast air-fuel mixing to speed up the combustion due to lower levels of turbulence. This is consistent with the non-EGR results, but the effects were even more pronounced for higher levels of EGR.

The response plots for the two methanol cases (standard- or wave-piston) were similar in terms of $\eta_{f,ig}$ and ISNOx levels over the investigated area. However, at high injection pressures and early timings, the wave piston performed better for ISNOx, with a peak at just over 4 g/kWh compared to slightly more than 7 g/kWh for the standard piston. Thermal NOx formation is a function of local temperature and residence time. Thus, it appears that the wave piston enabled significantly faster

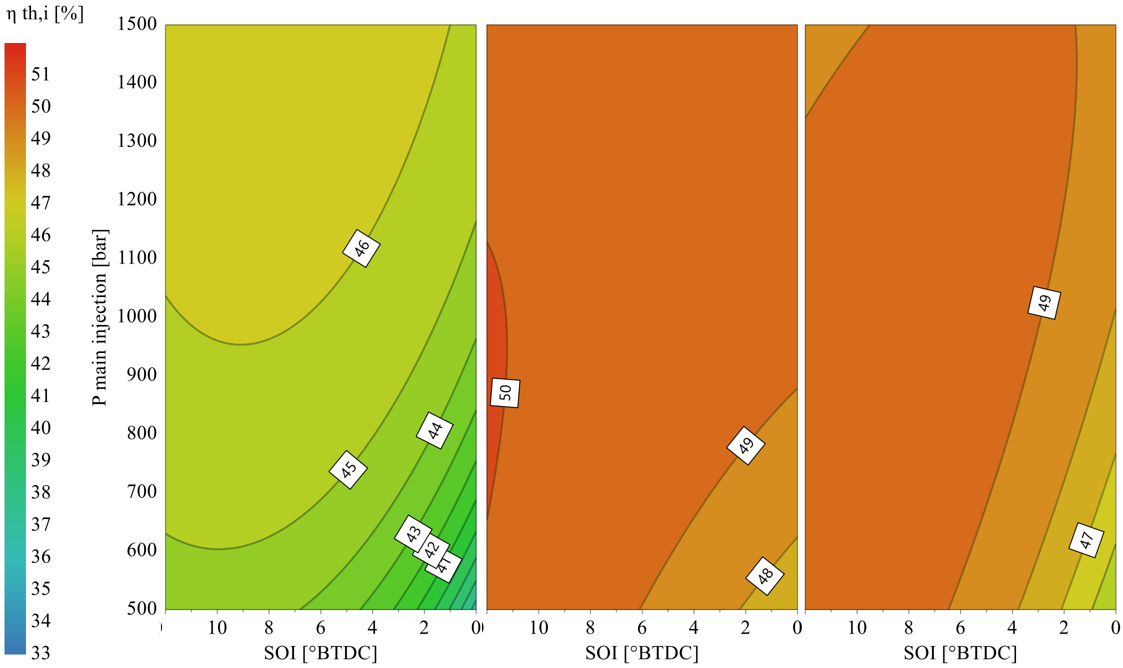

Figure 5.8: $\eta_{f,ig}$ DoE response plot for Diesel, methanol (both standard-piston) and methanol (wave-piston) at 1262 rpm, 172 Nm and 15 % EGR.

combustion, as shown in Figure 5.9. Overall, the wave piston supported shorter combustion durations. This indicates that the wave-shaped piston enhanced fuel-air mixing, as intended, and hence speeded up the combustion process.

Running an engine with EGR can cause soot, hydrocarbon (HC) and CO emissions to increase significantly. Linear regression response plots for soot are not shown here because the emissions for both methanol cases were extremely low, generally 40 times lower than for Diesel.

Other emissions, such as HCs and CO, may also be greatly affected by the use of EGR. However, the value-range for Diesel and methanol were significantly different. Therefore, it was impossible to plot them in a meaningful fashion. Table 5.3 gives an overview of the maximum and minimum values for all three cases. For non EGR cases, the values ranged from low at about 0.1 to high at about 0.8 g/kWh, with slight advantages shown by Diesel. The wave piston performed as well as the standard piston, but this changed with the introduction of EGR. For 15 % EGR, the CO levels increased to up to 20 g/kWh and at 30 % to 38 g/kWh for Diesel. This indicates very poor combustion. These high levels of CO were found with high EGR levels and late injection timing at low injection pressure. However, methanol performed significantly better, especially under high EGR conditions, when the CO level remained under 8 g/kWh. This was associated with a drop in efficiency in the same region, as discussed for Diesel but not as distinct. The wave piston performed slightly better under high EGR conditions for HC emissions, potentially due to increased air-fuel mixing.

The efficiencies with EGR were slightly lower overall compared to those recorded without EGR (Figure 5.4). This may be due to the lower availability of oxygen,

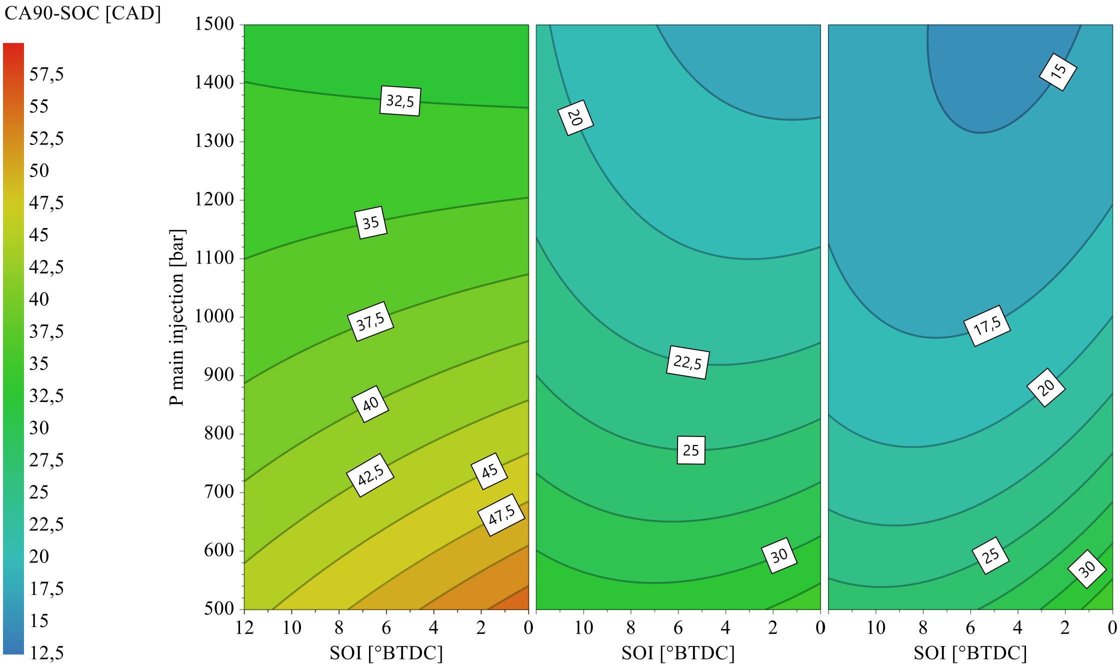

Figure 5.9: Combustion duration DoE response plot for Diesel, methanol (both standard-piston) and methanol (wave-piston) at 1262 rpm, 172 Nm and 15 % EGR.

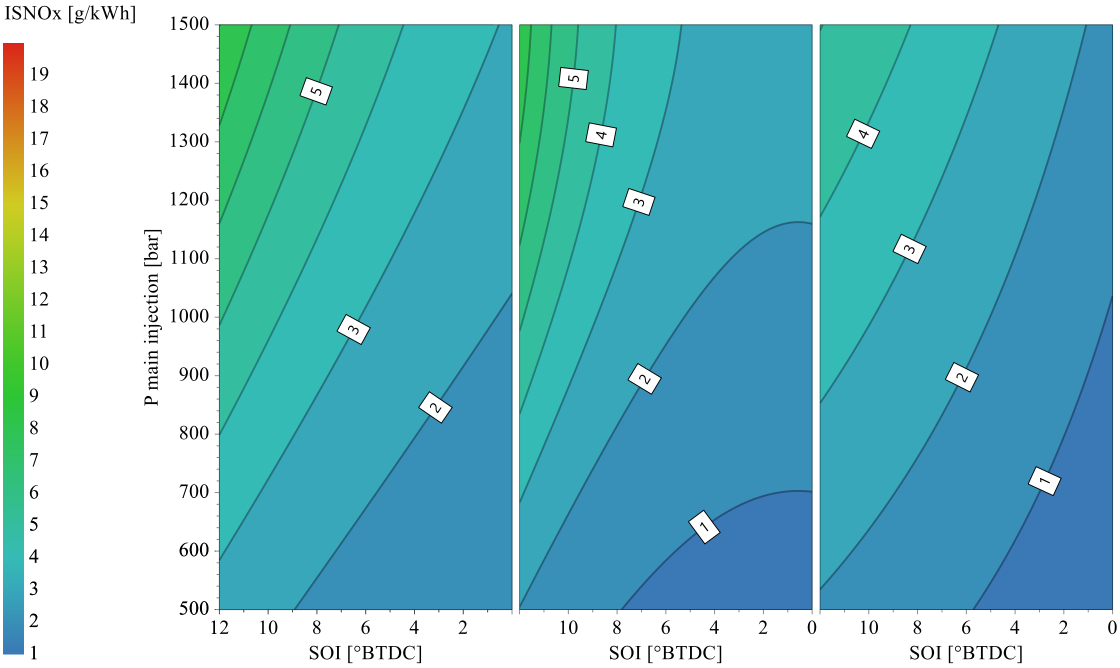

Figure 5.10: ISNOx DoE response plot for Diesel, methanol (both standard-piston) and methanol (wave-piston) at 1262 rpm, 172 Nm and 15 % EGR.

Table 5.3: HC and CO emissions from the DoEs of Diesel, methanol (both standard-piston and methanol (wave-piston), at 1262 rpm, 172 Nm and up to 30 % EGR.

Diesel			**Methanol**			**Methanol**			
non-EGR	low	high		low	high				Unit
CO	0.12	0.38	standard	0.09	0.14	wave	0.11	0.55	[g/kWh]
HC	0.12	0.38	standard	0.31	0.55	wave	0.18	0.80	[g/kWh]
EGR 15 %									
CO	0.17	20	standard	0.10	0.50	wave	0.14	1.40	[g/kWh]
HC	0.10	0.31	standard	0.20	0.50	wave	0.17	0.75	[g/kWh]
EGR 30 %									
CO	1.25	38	standard	0.24	7.30	wave	0.31	7.50	[g/kWh]
HC	0.1	0.25	standard	0.20	0.47	wave	0.07	0.18	[g/kWh]

which slowed down the combustion process, as shown in Figure 5.9 by the response plots of the combustion duration. A short duration close to the thermodynamically preferable position is desirable, but in this case it reduced thermal NOx (Figure 5.10).

5.2.3 Summary of DoE results

Summarizing the results from all DoEs, they generally followed the trends observed in single speed-load investigations. The investigated alcohol fuels outperformed Diesel when using the same setup and conditions for all significant parameters. The DoE results provided a more detailed picture on how the dual-fuel engine operates and suggested significant advantages of methanol, ethanol and E85 compared with Diesel. Methanol and ethanol did not show an absolute maximum for $\eta_{f,ig}$, whereas E85 did. The overall results, even though not all presented here, showed similar outcomes in terms of the performance of key parameters. The ISCO$_2$ emissions vs. ISNOx emissions for the three speed-loads measured during the DoE investigations are presented in the sub-figures of Figure 5.11 and illustrate the discussed superiority. At 1262 rpm and 172 Nm (Figure 5.11a), the CO$_2$ emissions were the lowest for methanol at NOx levels of less than 10 g/kWh, around 10 % lower than for Diesel. Ethanol had slightly higher CO$_2$ emissions, closely followed by E85. The differences mainly stemmed from higher thermal efficiencies but also a significantly lower mass-% of carbon in the alcohol fuels (Table 3.1). At 1508 rpm and 285 Nm, the trends were more pronounced. Methanol showed a significant advantage in terms of CO$_2$ and NOx emissions. Interestingly, the difference between ethanol and E85 was more evident. This can be attributed to a higher carbon content as well as 15 % gasoline of E85 were gasoline. In the low load case at 871 rpm and 86 Nm (Figure 5.11c), a similar trend was observed. Methanol performed the best, whereas ethanol and E85 were similar, with small advantages in terms of CO$_2$ emissions for ethanol.

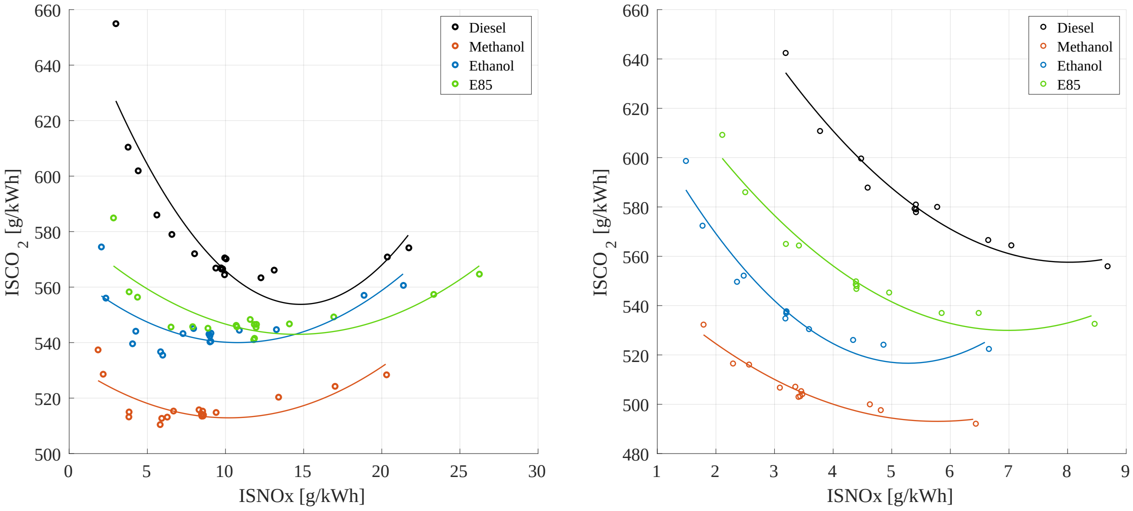

(a) ISCO2 vs ISNOx emissions for 1262 rpm and 172 Nm.

(b) ISCO2 vs. ISNOx emissions for 1508 rpm and 285 Nm.

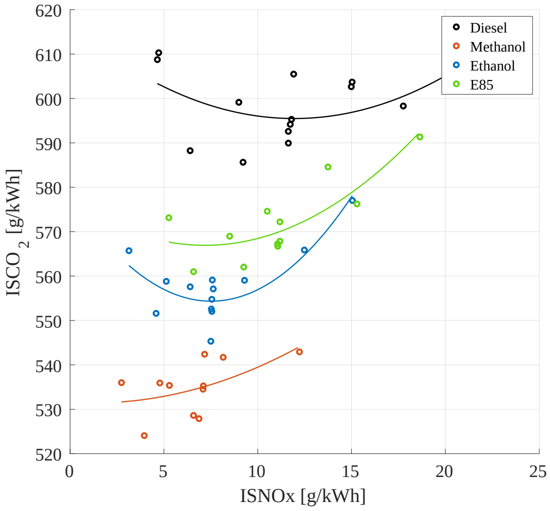

(c) ISCO2 vs. ISNOx emissions for 871 rpm and 86 Nm.

Figure 5.11: Summary of results from the DoEs at all three speed-load cases for ISCO2 vs. ISNOx emissions.

5.3 Wave Piston Results

This work expanded the investigation of the wave piston started in the DoE study. Methanol combustion using a standard piston was compared to methanol combustion using a wave piston and Diesel with a standard piston as a reference. All tests were conducted at 1250 bar injection pressure and the CA50 was targeted to be around 7.5 aTDC without and with 20 % EGR. The investigation was based on aRoHR curves. In this section, all relevant results are presented in spider plots and the focus of the discussion is on the results for the wave piston compared to those for the standard piston.

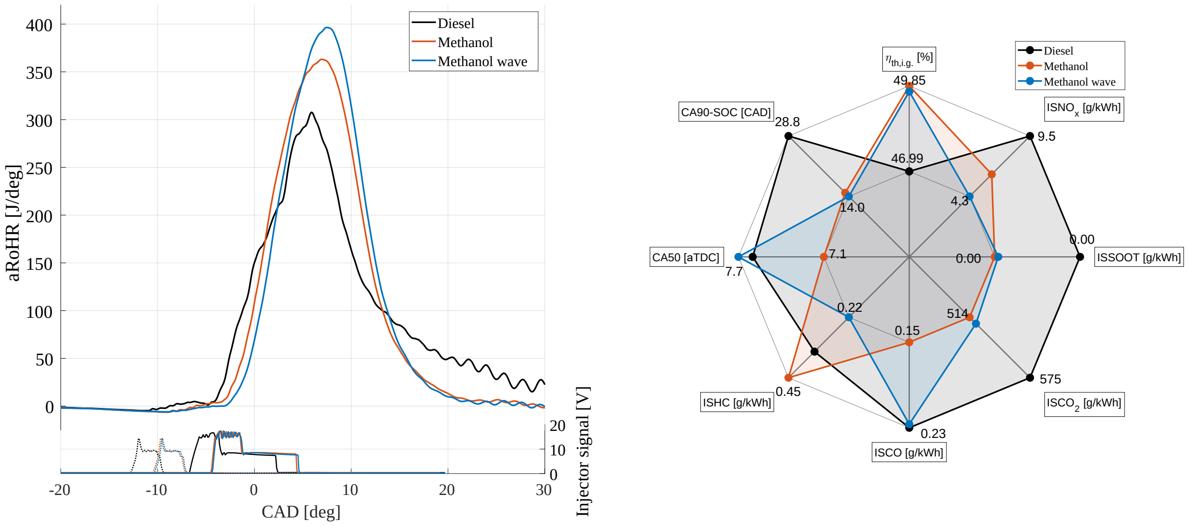

(a) aRoHR curves.

(b) Spider plot of the most important results.

Figure 5.12: aRoHR curves, emissions, engine, and combustion data for Diesel, methanol (both standard-piston) and methanol (wave-piston) at 1262 rpm, 172 Nm and 1250 bar injection pressure.

Figure 5.12a shows aRoHR curves calculated for the three fuels. The HR curve for methanol with a wave piston had a slightly longer ignition delay with the fuels being injected at almost the same time. This could indicate that the ignition process induced by the pilot was sufficient but with a possibly slightly different heat distribution around the main injector nozzle tip, causing a slightly longer delay. The combustion speed was the same for both methanol cases, since the slope of the HR curves was almost identical. The peak of methanol with a wave piston was significantly higher, indicating faster fuel-air mixing. After the EOI, both HR curves declined in a similar fashion, ending in a marginally shorter tail for methanol with the wave piston.

Additional information can be found in Figure 5.12b. The $\eta_{f,ig}$ was nearly equally high (just less of 50 %) for both types of piston, whereas ISNOx was significantly lower for the wave piston. The delay at the beginning of the combustion could indicate a lower ambient temperature at the SOI. Soot and CO_2 emissions were very similar and both were lower than for Diesel. CO emissions for the wave piston were slightly higher, but HC emissions were lower. Additionally, the combustion duration was slightly lower for the wave piston that the standard piston, which is consistent with the findings from the DoE and HR curves. The wave-piston was used in a study with longer chain alcohols and conducted by Zhang et. al. It was reported that most emissions were generally lower or equal to the Diesel reference, which corresponds to the results found here [59].

Figure 5.13a shows the aRoHR for 20 % EGR. The findings in terms of HR shape and orientation were similar to the non-EGR case. However, the results depicted in the spider plot of Figure 5.13b show a lower $\eta_{f,ig}$ for the wave piston case, probably due to the slightly later CA50. Other results were in line with the non-EGR cases.

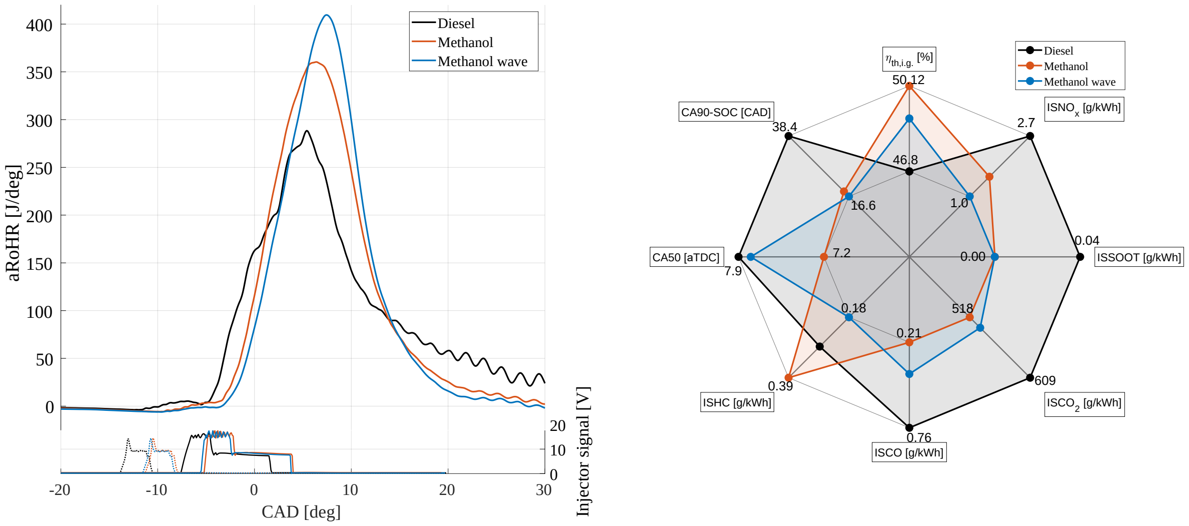

(a) aRoHR curves. (b) Spider plot of the most important results.

Figure 5.13: aRoHR curves, emissions, engine, and combustion data for Diesel, methanol (both standard-piston) and methanol (wave-piston) at 1262 rpm, 172 Nm, 20 % EGR and 1250 bar injection pressure.

5.4 Influence of the Hydraulic Flow on Methanol Dual-Fuel Combustion

One of the key elements of a DI ICE, especially Diesel engines, is the fuel injection process. Changing the hole size, number, cone angle and injector hydraulic flow can have a large impact on the fuel-air mixing process, and hence efficiency of an engine and its emissions. In Paper I, the liquid and vapor phase of ethanol high pressure sprays is described. The investigation was conducted using a single hole injector with a hole size equivalent to one of the eight holes of the 4.6 l/min injector mainly used throughout the project. This flow number was selected to compensate the lower LHV of methanol compared with a 2.3 l/min Diesel injector. A short test campaign was conducted to explore the effects of a lower, closer to a Diesel injector, hydraulic flow nozzle on the methanol dual-fuel combustion. A low and a medium speed-load point were investigated, by targeting a similar specific energy injected per CAD was targeted together with a desired CA50 between 6 and 7 °aTDC. The injection pressure was limited to 2000 bar. Additionally, the RSCs were investigated as a high speed-load point. the injection pressures and specific energies are summarized in Tables 5.4, 5.5 and 5.6. First, the aRoHR of each point is discussed together with a spider plot summarizing the main results and concluding with an energy balance investigation.

5.4.1 1262 rpm 172 Nm

Figure 5.15 shows the results recorded for the medium speed-load case at 1262 rpm and 172 Nm. The specific energy injected was very similar for all cases investigated.

The ignition delay was almost negligible and of the same order of magnitude for all three nozzles. The Diesel and the 4.6 l/min flow injector show similar HR curve shapes, with a clearly visible free-flame phase in the beginning, followed by the flame-wall interaction phase about half way to the peak of the HR where the combustion speed slows slightly, followed by a flame-flame interaction phase close to peak HR. Those phases and their correlations with the presented HR curves were described in more detail in Paper IV and confirmed by CFD simulations.

Table 5.4: Settings investigated for comparing the methanol dual-fuel combustion for different hydraulic flows, 3.0 l/min, 4.6 at a medium speed-load of 1262 rpm and 172 Nm.

Fuel	**Flow [l/min]**	**P_{main} [bar]**	**Spec. energy [J/CAD]**
Diesel	2.3	750	409
Methanol	3.0	2000	401
Methanol	4.6	700	398

The methanol dual-fuel combustion of the low flow number injector does not show those distinct points in the HR curve. The slope of the aRoHR curve is significantly steeper, since it starts later and reaches its peak earlier compared to the other two HR curves. A possible explanation is the very large difference in injection pressure, 2000 bar to around 700 for the Diesel and standard methanol injector. Figure 5.14, shows the maximum and averaged turbulent kinetic energy for the two methanol nozzles derived from CFD simulations. It is evident that the higher injection pressure combined with a lower flow number enhanced the fuel-air mixture and increased combustion speed. The 3.0 l/min nozzle HR curve reached a plateau at about 350 J/deg where the injected amount of energy and heat released were in a kind of equilibrium. The 50 J/deg difference between the injected energy and peak value of the HR curve stemmed mainly from energy going into evaporating liquid fuel and heat and other losses.

The injector closing events behaved similarly, as shown by the distance between the end of the injector current signal and the HR curve starting to have a significantly negative slope after the EOI. The HR tail was much shorter for 3.0 l/min nozzle. A possible explanation for this is that after the EOI, less unreacted fuel remained around the nozzle tip and burned off quicker once evaporated. There was no effect on soot emissions owing to the extremely low levels for methanol in general. Figure 5.15b shows the most interesting results of this comparison. Both nozzles with methanol outperformed that with Diesel, in line with previous investigations. $\eta_{f,ig}$ differs significantly, with 51 % being the highest for the 4.6 l/min flow nozzle and 48.5 % for the low flow nozzle. Interestingly, the combustion duration was significantly shorter for the latter, which would suggest an opposing result. A possible explanation can be increased heat losses combined with a slightly less favourable CA50. The energy balance in Figure 5.18a shows that the share of energy lost through heat losses, friction and others was significantly larger for the small flow number injector. Assuming that friction and other losses of the system were almost constant the remaining losses were heat losses. The energy leaving the system through exhaust gases were very similar for all three cases at this speed-load. The emission results

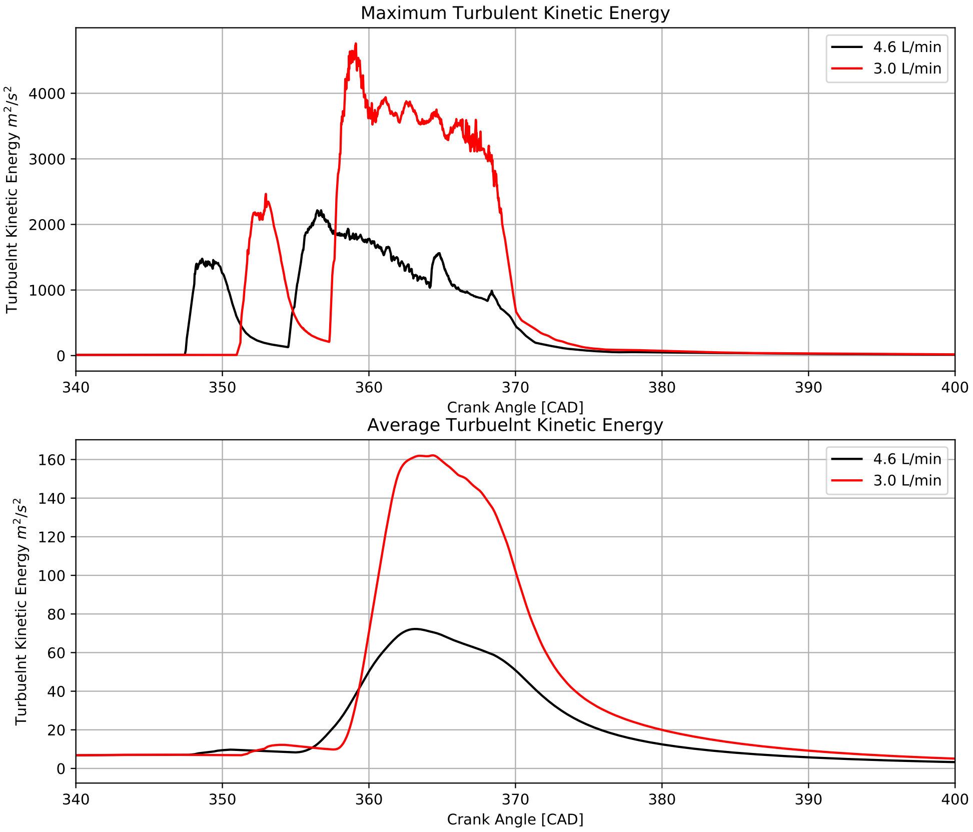

Figure 5.14: Maximum and averaged turbulent kinetic energy for 3.0 l/min and 4.6 l/min flow injector nozzles at 2000 and 700 bar injection pressure respectively [34].

were very similar for the two methanol cases. NOx was slightly elevated, but can be explained by the higher combustion temperatures due to the faster combustion induced by high injection pressure turbulence and higher turbulence. CO and HC emissions were slightly lower for the small nozzle. An investigation on nozzle size effects with Diesel fuel suggests, that those emissions reduce with smaller orifice diameter [4].

5.4.2 871 rpm 86 Nm

Figure 5.16 shows the results recorded for the low speed-load case at 871 rpm and 86 Nm. Fuel quantities injected were significantly smaller compared with the medium load cases, however, the injected energy per CAD was significantly larger due to similar injection pressures at low engine speed, as shown in Table 5.5.

As a result the earlier mentioned different phases of the combustion are not easily distinguishable, even for Diesel. This was due to the short injection duration and

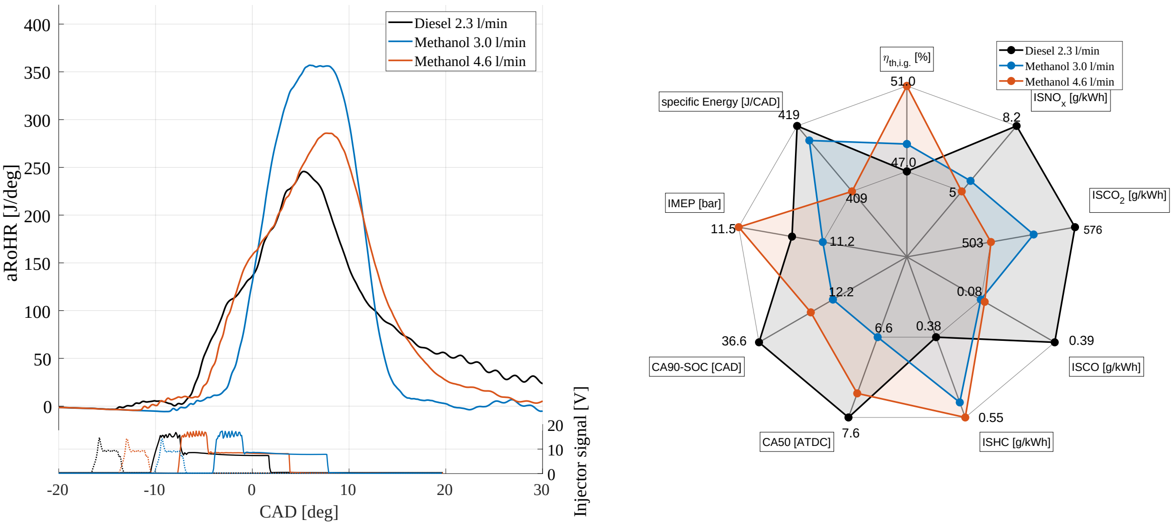

(a) aRoHR curves. (b) Spider plot of the most important results.

Figure 5.15: aRoHR curves, emissions, engine, and combustion data for Diesel and methanol at 1262 rpm, 172 Nm and different flow number injectors.

Table 5.5: Settings investigated for comparing the methanol dual-fuel combustion for different hydraulic flows, 3.0 l/min, 4.6 at a medium speed-load of 871 rpm and 86 Nm.

Fuel	**Flow [l/min]**	$\mathbf{P}_{main}$ **[bar]**	**Spec. energy [J/CAD]**
Diesel	2.3	750	564
Methanol	3.0	2000	552
Methanol	4.6	750	600

fast combustion at this speed-load, which did not allow the HR being influenced by flame-wall and flame-flame interaction phases. The aRoHR for the two methanol cases start off with a very similar combustion speed, both faster than Diesel.

However, the injection pressure for the 3.0 l/min nozzle was significantly higher, creating a stronger turbulences and therefore better fuel-air mixing and a faster combustion. This is reflected by the slightly steeper rise of the HR curve and the significantly higher peak at about 380 J/CAD. The 4.6 l/min HR curve peaks at a much lower 275 J/CAD and Diesel even lower with 200 J/CAD. The tail of both methanol HR curves were shorter than Diesel, with a significantly shorter tail for the small flow number injector running on methanol. As a result, the combustion duration was the shortest for the 3.0 due to the faster combustion mainly driven by the high injection pressure. The $\eta_{f,ig}$ was slightly lower for the 3.0, but that can be explained by the marginally less favourable CA50 and slightly higher heat losses visible in Figure 5.18c. Figure 5.16b summarises all other relevant results. ISNOx, ISCO$_2$, ISCO and ISHC followed the same trend as under the medium speed-load conditions.

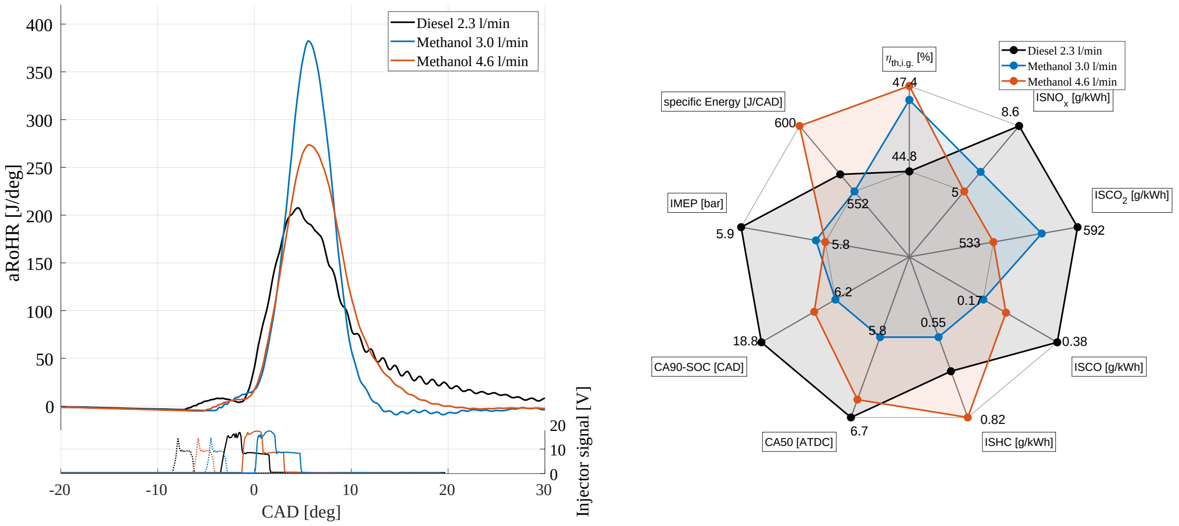

(a) aRoHR curves.

(b) Spider plot of the most important results.

Figure 5.16: aRoHR curves, emissions, engine, and combustion data for Diesel and methanol at 871 rpm, 86 Nm and different flow number injectors.

5.4.3 1400 rpm 305 Nm

Figure 5.17 shows the aRohR curves of all RSCs and the mean results of the most important emissions, engine and combustion data for Diesel and methanol with two different flow number nozzles. Table 5.6 shows the main settings for comparing the cases.

Table 5.6: Settings investigated for comparing the methanol dual-fuel combustion for different hydraulic flows, 3.0 l/min, 4.6 at a medium speed-load of 1400 rpm and 305 Nm.

Fuel	**Flow [l/min]**	**P_{main} [bar]**	**Spec. energy [J/CAD]**
Diesel	2.3	1250	537
Methanol	3.0	1500	316
Methanol	4.6	1250	486

The specific energy injected were significantly different in this investigation, but the RSCs can still give valuable information on the use of a lower flow number injector with methanol dual-fuel.

Figure 5.17a shows the HR curves of all RSC cases run. The variations between single runs of the RSCs were generally small. The lower injected energy per CAD is clearly visible as the peak of the 3.0 l/min curve peaks significantly lower than even Diesel. The lower peak was compensated by a longer overall combustion duration. However, the 3.0 l/min configuration outperformed Diesel in terms of $\eta_{f,ig}$ and ISNOx emissions, slightly lower than the 4.6 l/min. The energy balance of theses cases presented in Figure 5.18b, shows that the energy loss was slightly higher for 3.0 compared to 4.6, which can explain the slightly lower efficiency. The results of the RCSs show good repeatability with small errors in general.

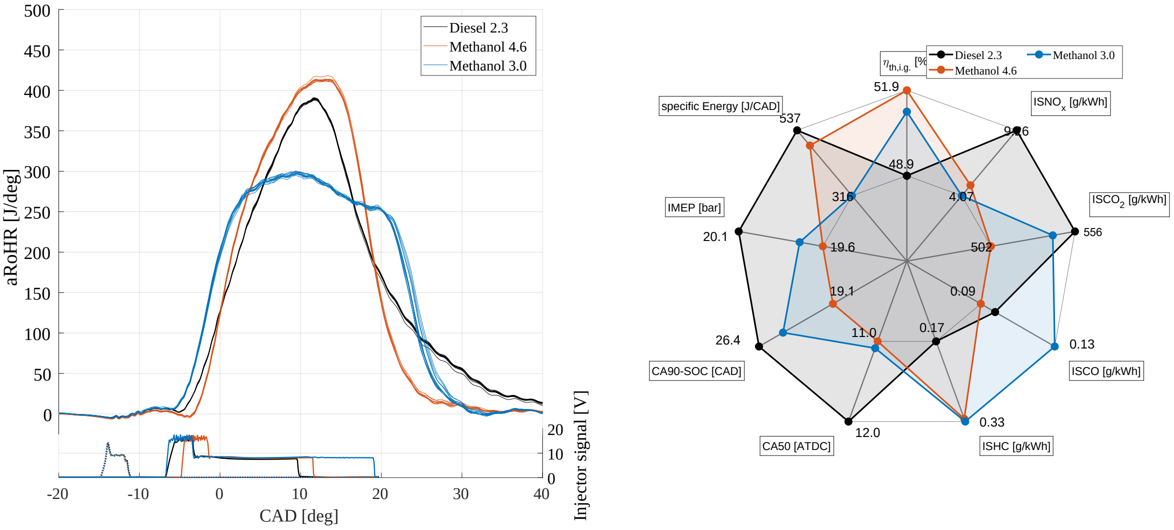

(a) aRoHR curves.

(b) Spider plot of the most important results.

Figure 5.17: Single aRoHR curves, emissions, engine, and combustion data for Diesel and methanol at 1400 rpm, 305 Nm at the RSC and different flow number injectors.

5.4.4 Energy balances

Figure 5.18 shows the energy balances of all three cases discussed in this subchapter. The energy going into the exhaust was almost constant within each speed-load case, but slightly higher for Diesel, due to higher exhaust gas temperatures. However, the difference of energy losses (heat, friction and other losses) and energy in the exhaust was significant among the speed-load points. A lower speed and load had a smaller portion of the energy leaving the system with the exhaust gases, up to 23 %. With around 30 %, a larger portion can be attributed to thermal, friction and other losses. At high speed and load this turns to the opposite with around 35 % of energy leaving the systems with the exhaust gases and 15 to 20 % that can be allocated to energy losses. These observations correlate with results in literature [17]

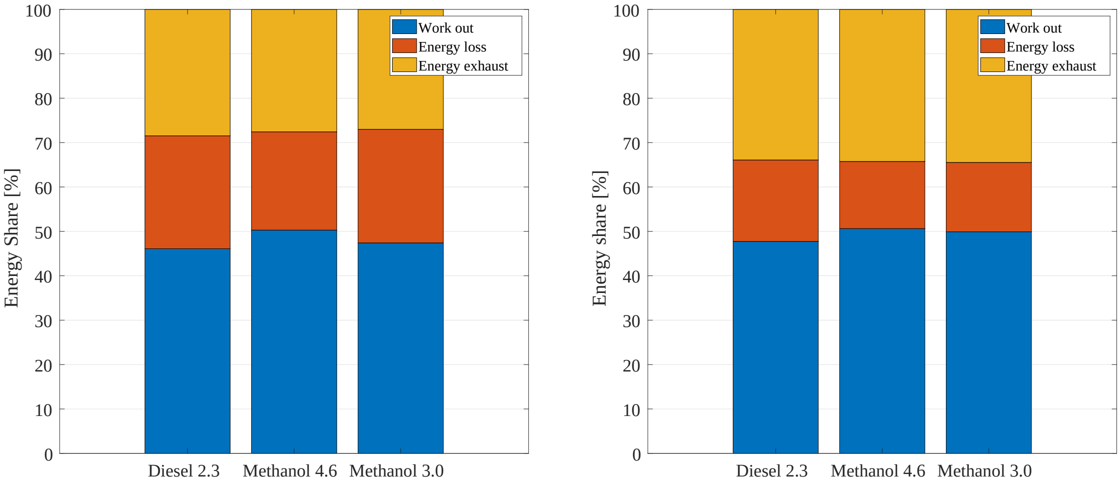

(a) Specific energy balance for 1262 rpm and 172 Nm.

(b) Specific energy balance for 1400 rpm and 305 Nm.

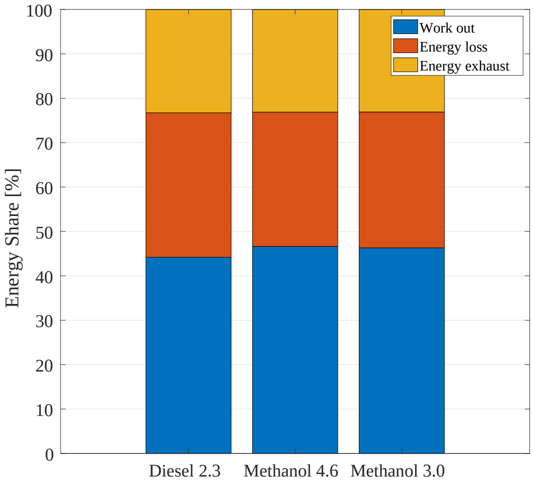

(c) Specific energy balance for 871 rpm and 86 Nm.

Figure 5.18: Energy Balances of the three load cases investigated, showing the work out, energy losses accumulate heat losses, friction and e.g. blow and energy leaving the system through the exhaust gases; Mean values of min. 9 runs were used for the RSC.

Chapter 6

Conclusions

This chapter summarizes and concludes the work conducted during the course of this project. The first experimental campaign was a spray investigation on a high pressure/high temperature chamber and the main results were published in Paper I. The second experimental campaign involved SCE tests and was divided into several investigations. The main results are published in Papers II to IV and the Results and Discussion section (Chapter 5) of this thesis.

6.1 Conclusions from spray experiments

The main conclusion from the spray experiments was that a standard HD Diesel common rail system can be adapted, with few changes, to be used with ethanol and up to injection pressures of 2200 bar. The results obtained were in line with other studies, showing that the injection pressure had only a minor effect on the liquid penetration length of the injection. Additionally, a strong correlation between the liquid length and ambient gas temperature was shown. In comparison with Diesel fuel, the liquid length was shorter and the cone angle smaller, which indicates an equivalently good fuel-air mixing process.

6.2 Conclusions from SCE Experiments

During the course of the first experimental investigation of the dual-fuel setup with methanol, it was concluded that the dual injector arrangement created a stable and repeatable environment for methanol-Diesel dual-fuel combustion (Paper II). Under similar conditions and on the same system, combustion with conventional Diesel was outperformed by that with the alternative fuels in terms of $\eta_{f,ig}$ and brake-specific NOx emissions. Soot emissions were also significantly lower than for Diesel. However, limiting factors on the mechanical side of the system were identified as the peak cylinder pressure and peak pressure rise rates, particularly at high load points.

The work reported in Paper III utilized the stable ignition conditions of methanol with ignition improver to explore a single-fuel option on the SCE. Methanol was therefore blended with 5 % polyethylene glycol and a pilot-main injection strategy was adopted to obtain stable ignition with modest CR. Additionally, ethanol, which is currently used commercially in this type of engine, was investigated with a standard compression ratio piston and a CR20 piston. The results showed that the standard piston did not always manage to provide ambient conditions at the SOI to stably ignite the blends. These issues were overcome at CR20, confirming studies on the use of low carbon alcohol fuels in CI engines. High thermal indicated efficiencies were reached on CR20 with a pilot-main injection strategy. In general, the controllability was more difficult in comparison with the dual-fuel concept proposed. Additionally, even higher peak pressure rise rates were recorded at lower medium load cases, putting a higher level of stress on the system.

Paper IV presented a comprehensive analysis of the dual-injector concept based on a thorough investigation into different speed-loads and EGR as a NOx mitigation strategy. The main conclusion made in the publication was that the concept worked well over the investigated speed-load range. Both, methanol and ethanol significantly outperformed Diesel in terms of $\eta_{f,ig}$, soot, NOx and tailpipe CO_2 emissions, while maintaining low levels of HCs and CO. The fuel substitution ratios were over 95 % and mainly responsible for the lower CO_2 tailpipe emissions. Use of a 100 % renewable alcohol fuel could reduce the net CO_2 emissions even further. The peak pressure rise rate did not pose a problem and the peak cylinder pressure issue could be resolved by using an engine that allows higher peak pressures, which are available today.

Additionally, E85 was investigated as an additional already available fuel alternative. The main conclusions drawn from the DoE investigations were that methanol and ethanol showed large advantages over Diesel, not only at single operating points but also over a whole range of different conditions. The main conditions investigated were the injection pressure of the main fuel, SOI of the main fuel and EGR for NOx mitigation. E85 performed significantly better than Diesel in terms of $\eta_{f,ig}$, but higher NOx emissions were found under certain conditions. However, this trend was not significant when comparing the results of tailpipe CO_2 over NOx emissions. Methanol showed the most promising overall performance.

Several single components, such as Volvo's wave piston and main injectors with different flow rates, were also investigated. The wave piston performed equally well in terms of $\eta_{f,ig}$ and slightly better regarding NOx emissions. The results from the injector study showed that the chosen 4.6 l/min injector gave the best results at the investigated speed-load cases. The lower flow number injector would be impossible to use during full load operation. The higher flow rate injector might offer some benefits at high loads but would be difficult to operate at very low or idle operation conditions.

6.3 Conclusions summary

The proposed dual-fuel concept tested on a single cylinder engine performed well with all alcohol fuels used compared with Diesel. Ignition of the alcohol fuels was not a problem under normal conditions and the combustion stability and controllability of the system was always good. At high levels of EGR, ignition became harder, but this could be resolved by slightly increasing the Diesel pilot.

Is it possible to have a true alcohol flexible dual-fuel combustion system?

Yes it is possible. It was shown, that all tested alcohols worked very well in the system. It can be assumed that blends of these alcohols and other alcohols with similar properties, or even gasoline like fuels, can be used with the presented concept.

What advantages and challenges, connected to the alcohol flexible dual-fuel direct injection engine, can be identified from experimental studies?

- It reduces all relevant pollutants significantly.
- The fuel substitution ratio is very high over 95 % in all cases and for high load cases over 98 % outperforming PFI and other premixed dual-fuel combustion strategies.
- All of the hardware is already available, but some adjustments have to be made.
- Theoretically it is possible to operate the system on 100 % renewable fuels, by using an alcohol from renewable sources and HVO.
- The technology adds parts to an already complex system.
- Exhaust gas temperatures are generally lower, can cause difficulties for the exhaust gas aftertreatment system.
- Legislation that focusses on reducing CO_2 on a tank-to-wheel approach will be tough to meet, even with a low carbon fuel.

How large is the carbon dioxide CO_2, PM and NOx reduction potential from a flexfuel engine run on various alcohol fuels compared with Diesel? (best case alcohol to best case Diesel)

- CO_2 reduction potential of up to 120 g/kWh, which corresponds to a reduction of up to 25 % under optimal conditions without EGR.
- NOx reduction potential of up to 5 g/kWh, which corresponds to a reduction of up to 45 % under similar conditions without EGR
- PM reduction potential of up to 0.003 g/kWh, which corresponds to a reduction of a factor of 45 and more.

Chapter 7

Outlook

This chapter gives an outlook on work needed to further develop this technology toward commercial use. The conclusions drawn show that this technology has potential to be further developed to reduce GHGs and local emissions from HD internal combustion engines. The next steps in the development will require further expansion of the steady-state points over the whole operating range of the engine in order to generate a comprehensive engine map. The results could be used to create and validate CFD models, which then in turn may assist with optimizing different hardware components and the combustion chamber design. Important topics to investigate include transient operations of the system, cold start conditions and how this type of engine could be integrated into an existing powertrain.

Bibliography

[1] Kazuhiro Akihama et al. "Mechanism of the Smokeless Rich Diesel Combustion by Reducing Temperature". In: 2001.724 (2001). ISSN: 0148-7191. DOI: `10.4271/2001-01-0655`.

[2] Malin Alriksson, Tanja Rente, and Ingemar Denbratt. "Low Soot , Low NOx in a Heavy Duty Diesel Engine Using High Levels of EGR". In: *SAE International* 724 (2005).

[3] I. M. Atadashi, M. K. Aroua, and A. Abdul Aziz. "High quality biodiesel and its diesel engine application: A review". In: *Renewable and Sustainable Energy Reviews* 14.7 (2010), pp. 1999–2008. ISSN: 13640321. DOI: `10.1016/j.rser.2010.03.020`.

[4] Pär Bergstrand. *Small Orifices - Diesel Combustion and Spray investigations.* Doktorsavhandlingar vid Chalmers tekniska högskola. Ny serie: 2000. Chalmers University of Technology, 2003.

[5] K. Browne, I. Partridge, and G. Greeves. "Fuel Property Effects on Fuel/Air Mixing in an Experimental Diesel Engine". In: *SAE Technical Paper* (1986). DOI: `10.4271/860223`.

[6] Bundesgesetzblatt Jahrgang 2006 Teil 1. *Verordnung zum Erlass und zur Änderung von Vorschriften über die Kennzeichnung emissionsarmer Kraftfahrzeuge*).* 2006.

[7] John E. Dec, Yi Yang, and Nicolas Dronniou. "Boosted HCCI - Controlling Pressure-Rise Rates for Performance Improvements using Partial Fuel Stratification with Conventional Gasoline". In: *SAE International Journal of Engines* 4.1 (2011), pp. 2011–01–0897. ISSN: 1946-3944. DOI: `10.4271/2011-01-0897`.

[8] Chengjun Du, Mats Andersson, and Sven Andersson. "An analysis of image evaluation procedures for measurments of diesel spray characteristics". In: *ILASS – Europe 2014 conference paper* (2014).

[9] Jan Eismark. *The role of piston bowl shape in controlling soot emissions from heavy-duty diesel engines.* Doktorsavhandlingar vid Chalmers tekniska högskola. Ny serie: 4470. Chalmers University of Technology, 2018.

[10] Jan Eismark et al. "Role of late soot oxidation for low emission combustion in a diffusion-controlled, High-EGR, heavy duty diesel engine". In: *SAE Technical Papers* 4970 (2009), pp. 1–15. ISSN: 26883627. DOI: `10.4271/2009-01-2813`.

[11] European Commission. “A European Strategy for Low-Emission Mobility, SWD 244 final”. In: (2016), p. 13.

[12] European Commission. *CO 2 emission standards for heavy-duty vehicles Mobility Packages I-III : an integrated approach.* 2019. URL: `https://ec.europa.eu/clima/sites/clima/files/transport/vehicles/heavy/docs/hdv%7B%5C_%7Dco2%7B%5C_%7Dstandards%7B%5C_%7Den.pdf` (visited on 07/23/2020).

[13] European Commission. *EU Reference Scenario 2016: Energy, Transport and GHG emissions trends to 2050.* 2016, p. 27. ISBN: 978-92-79-52373-1. DOI: `10.2833/9127`.

[14] K. R. Gerdes and G. J. Suppes. “Miscibility of ethanol in diesel fuels”. In: *Industrial and Engineering Chemistry Research* 40.3 (2001), pp. 949–956. ISSN: 08885885. DOI: `10.1021/ie000566w`.

[15] Hannes Gruber et al. “Fischer-Tropsch products from biomass-derived syngas and renewable hydrogen”. In: *Biomass Conversion and Biorefinery* (2019). ISSN: 21906823. DOI: `10.1007/s13399-019-00459-5`.

[16] Alan C. Hansen, Qin Zhang, and Peter W.L. Lyne. “Ethanol-diesel fuel blends - A review”. In: *Bioresource Technology* 96.3 (2005), pp. 277–285. ISSN: 09608524. DOI: `10.1016/j.biortech.2004.04.007`.

[17] John B Heywood. *Internal Combustion Engine Fundementals.* Vol. 21. 1988, p. 930. ISBN: 007028637X. DOI: `10987654`.

[18] Healt Effects Institute. “Diesel Exhaust : A Critical Analysis of Emissions, Exposure, and Health Effects”. In: (1995), pp. 1–294.

[19] IPCC et al. *Climate Change 2014: Mitigation of Climate Change. Contribution of Working Group III to the Fifth Assessment Report of the Intergovernmental Panel on Climate Change.* Cambridge University Press, Cambridge, United Kingdom and New York, NY, USA, 2014, p. 1454. ISBN: 9781107654815. DOI: `10.1017/CBO9781107415416`. arXiv: `arXiv:1011.1669v3`.

[20] Takeyuki Kamimoto and Myurng Hoan Bae. “High combustion temperature for the reduction of particulate in diesel engines”. In: *SAE Technical Papers* (1988). ISSN: 26883627. DOI: `10.4271/880423`.

[21] M. Krishnamoorthi et al. “A review on low temperature combustion engines: Performance, combustion and emission characteristics”. In: *Renewable and Sustainable Energy Reviews* 116.October (2019), p. 109404. ISSN: 18790690. DOI: `10.1016/j.rser.2019.109404`.

[22] Prommes Kwanchareon, Apanee Luengnaruemitchai, and Samai Jai-In. “Solubility of a diesel-biodiesel-ethanol blend, its fuel properties, and its emission characteristics from diesel engine”. In: *Fuel* 86.7-8 (2007), pp. 1053–1061. ISSN: 00162361. DOI: `10.1016/j.fuel.2006.09.034`.

[23] Erik Lewenhaupt and Stena Group. “METHANOL - A future fuel for shipping”. In: November (2015).

[24] W.G. Linstrom, P.J. Mallard. *NIST Standard Reference Database Number 69, Chemistry WebBook*. 2020. DOI: `https://doi.org/10.18434/T4D303`. URL: `http://webbook.nist.gov/cgi/cbook.cgi?Name=N2&Units=SI&cTG=on` (visited on 09/27/2020).

[25] Julian A Lorusso and Harry A Cikanek. "Direct Injection Ignition Assisted Alcohol Engine". In: *SAE Technical Paper* (1988). DOI: `10.4271/880495`.

[26] J. A. Mäder et al. "Evidence for the effectiveness of the Montreal Protocol to protect the ozone layer". In: *Atmospheric Chemistry and Physics* 10.24 (2010), pp. 12161–12171. ISSN: 16807316. DOI: `10.5194/acp-10-12161-2010`.

[27] Fredric C. Menz and Hans M. Seip. "Acid rain in Europe and the United States: An update". In: *Environmental Science and Policy* 7.4 (2004), pp. 253–265. ISSN: 14629011. DOI: `10.1016/j.envsci.2004.05.005`.

[28] Charles J Mueller and Mark P Musculus. "Glow Plug Assisted Ignition and Combustion of Methanol in an Optical DI Diesel Engine". In: 724 (2001). DOI: `10.4271/2001-01-2004`.

[29] Karin Munch and Tankai Zhang. "A Comparison of Drop-In Diesel Fuel Blends Containing Heavy Alcohols Considering Both Engine Properties and Global Warming Potentials". In: *SAE Technical Papers* 2016-Octobeer (2016). ISSN: 01487191. DOI: `10.4271/2016-01-2254`.

[30] Jeffrey Naber and Dennis L. Siebers. "Effects of Gas Density and Vaporization on Penetration and Dispersion of Diesel Sprays". In: 412 (1996). ISSN: 0148-7191. DOI: `10.4271/960034`.

[31] Gary D. Neely et al. "New Diesel Emission Control Strategy to Meet US Tier 2 Emissions Regulations". In: 2005.724 (2005). ISSN: 0148-7191. DOI: `10.4271/2005-01-1091`.

[32] Christof Noehre et al. "Characterization of Partially Premixed Combustion". In: *SAE Technical Paper, 2006-01-3412* 724 (2006), pp. 776–790. DOI: `10.4271/2006-01-3412`.

[33] Michel Noussan, Manfred Hafner, and Simone Tagliapietra. *The Future of Transport Between Digitalization and Decarbonization*. 2020. ISBN: 978-3-030-37965-0. DOI: `10.1007/978-3-030-37966-7`.

[34] Andreas Nygren. "personal communication". 2020.

[35] Tamilselvan Pachiannan et al. "A literature review of fuel effects on performance and emission characteristics of low-temperature combustion strategies". In: *Applied Energy* 251.301 (2019), p. 113380. ISSN: 03062619. DOI: `10.1016/j.apenergy.2019.113380`.

[36] Vinícius B. Pedrozo, Ian May, and Hua Zhao. "Exploring the mid-load potential of ethanol-diesel dual-fuel combustion with and without EGR". In: *Applied Energy* 193 (2017), pp. 263–275. ISSN: 03062619. DOI: `10.1016/j.apenergy.2017.02.043`.

[37] Vinícius B. Pedrozo et al. “High efficiency ethanol-diesel dual-fuel combustion: A comparison against conventional diesel combustion from low to full engine load”. In: *Fuel* 230.May (2018), pp. 440–451. ISSN: 00162361. DOI: `10.1016/j.fuel.2018.05.034`.

[38] Lyle M. Pickett and Dennis L. Siebers. “Non-sooting, low flame temperature mixing controlled DI diesel combustion”. In: *SAE transactions* 724 (2004). ISSN: 0096-736X. DOI: `10.4271/2004-01-1399`.

[39] Josefine Preuß, Karin Munch, and Ingemar Denbratt. “Performance and emissions of long-chain alcohols as drop-in fuels for heavy duty compression ignition engines”. In: *Fuel* 216.September 2017 (2018), pp. 890–897. ISSN: 00162361. DOI: `10.1016/j.fuel.2017.11.122`.

[40] Rolf D. Reitz and Ganesh Duraisamy. “Review of high efficiency and clean reactivity controlled compression ignition (RCCI) combustion in internal combustion engines”. In: *Progress in Energy and Combustion Science* 46 (2014), pp. 12–71. ISSN: 03601285. DOI: `10.1016/j.pecs.2014.05.003`.

[41] Karsten Röpke and Carsten Von Essen. “DoE in engine development”. In: *Quality and Reliability Engineering International*. Vol. 24. 6. 2008, pp. 643–651. DOI: `10.1002/qre.941`.

[42] Michael Saccullo et al. “High Pressure Ethanol Injection under Diesel-Like Conditions”. In: *SAE Technical Paper 2017-01-0857* (2017). ISSN: 01487191. DOI: `10.4271/2017-01-0857.Copyright`.

[43] Sartorius Stedim Data Analytics. “User guide to MODDE 12 Version 12”. In: (2017), pp. 1–394.

[44] Waterfront Shipping. “Methanol-fueled vessels mark one year of safe, reliable, and efficient operations”. In: April 2017 (2017).

[45] D. L Siebers. “Scaling liquid-phase fuel penetration in diesel sprays based on mixing-limited vaporization”. In: *SAE technical paper* 724 (1999), pp. 01–0528. ISSN: 0148-7191. DOI: `10.4271/1999-01-0528`.

[46] Dennis L. Siebers. “Liquid-Phase Fuel Penetration in Diesel Sprays”. In: 724 (1998). ISSN: 0148-7191. DOI: `10.4271/980809`.

[47] Dennis L. Siebers and C.F. Edwards. “Autoignition of Methanol and Ethanol Sprays under Diesel Engine Conditions”. In: *SAE Technical Paper* (1987). DOI: `10.4271/870588`.

[48] S. N. Soid and Z. A. Zainal. “Spray and combustion characterization for internal combustion engines using optical measuring techniques - A review”. In: *Energy* 36.2 (2011), pp. 724–741. ISSN: 03605442. DOI: `10.1016/j.energy.2010.11.022`.

[49] Jonas Strömberg. “Bioethanol in heavy duty transport”. In: Stellenbish, South Africa: 20th International Symposium on Alcohol Fuels (ISAF), 2013.

[50] The European Parliament and the Council of the European Union. “Regulation (EU) 2019/1242 of the European Parliament and of the Council of 20 June 2019 Setting CO2 emission performance standards for new heavy-duty vehicles and amending Regulations (EC) No 595/2009 and (EU) 2018/956 of the European Parliament”. In: *Official Journal of the European Union* L 198.April (2019), pp. 202–240.

[51] Martin Tuner. “Review and Benchmarking of Alternative Fuels in Conventional and Advanced Engine Concepts with Emphasis on Efficiency, CO 2 , and Regulated Emissions”. In: *SAE Technical Paper* (2016). ISSN: 01487191. DOI: `10.4271/2016-01-0882`.

[52] et.al. Ullman Terry L. “Emissions from Direct-Injected Heavy-Duty Methanol-Fueled Engines (One Dual-Injection and One Spark-Ignited) and a Comparable Diesel Engine”. In: *SAE International* (1982). DOI: `10.4271/820966`.

[53] R. Vallinayagam et al. “Feasibility of using less viscous and lower cetane (LVLC) fuels in a diesel engine: A review”. In: *Renewable and Sustainable Energy Reviews* 51 (2015), pp. 1166–1190. ISSN: 18790690. DOI: `10.1016/j.rser.2015.07.042`.

[54] Sebastian Verhelst et al. “Methanol as a fuel for internal combustion engines”. In: *Progress in Energy and Combustion Science* 70 (2019), pp. 43–88. ISSN: 03601285. DOI: `10.1016/j.pecs.2018.10.001`.

[55] Johan Visser, Toshinori Nemoto, and Michael Browne. “Home Delivery and the Impacts on Urban Freight Transport: A Review”. In: *Procedia - Social and Behavioral Sciences* 125 (2014), pp. 15–27. ISSN: 18770428. DOI: `10.1016/j.sbspro.2014.01.1452`.

[56] Martin Wissink and Rolf Reitz. “Exploring the Role of Reactivity Gradients in Direct Dual Fuel Stratification”. In: *SAE International Journal of Engines* 9.2 (2016), pp. 2016–01–0774. ISSN: 1946-3944. DOI: `10.4271/2016-01-0774`.

[57] Martin Wissink and Rolf D. Reitz. “Direct Dual Fuel Stratification, a Path to Combine the Benefits of RCCI and PPC”. In: *SAE International Journal of Engines* 8.2 (2015), pp. 2015–01–0856. ISSN: 1946-3944. DOI: `10.4271/2015-01-0856`.

[58] J Zeldovich. “The Oxidation of Nitrogen in Combustion and Explosions”. In: *Acta Physicochimica URSS* 21.4 (1946), p. 218. ISSN: 0364-3417. DOI: `10.1515/9781400862979.364`.

[59] Tankai Zhang et al. “Effects of a wave-shaped piston bowl geometry on the performance of heavy duty Diesel engines fueled with alcohols and biodiesel blends”. In: *Renewable Energy* 148.x (2020), pp. 512–522. ISSN: 18790682. DOI: `10.1016/j.renene.2019.10.057`.